Pergamon

0042-6989(95)00086-0

Vision Res. Vol. 36, No. 1, pp. 117–147, 1996

0042-6989/96 $9.50 + 0.00

A Cell Model for the Detection of Local Image Motion on the Magnocellular Pathway of the Visual Cortex

SUSUMU KAWAKAMI,*† HIROAKI OKAMOTO*

Received 28 April 1994; in revised form 16 December 1994; in final form 27 February 1995

We propose that five types of cell on the magnocellular pathway of the visual cortex constitute a function hierarchy for detecting local image motion. Lateral geniculate nucleus cells and two simple cell types analyse one-dimensional velocities perpendicular to oriented components within a moving stimulus. Combining these velocities, a group of complex cells along a sine wave fire over the cell array. The amplitude and phase of the wave correspond to the local motion's speed and direction. A motion-detection cell in the middle temporal area then extracts the wave of activated complex cells to detect the motion. Applying Hough and inverse Hough transforms and Reichardt's spatio-temporal correlation to the hierarchy, we modeled these cell types as a series of formulas that represent the synaptic functions of neurons. The modeled cells reflect the response to various stimuli in actual cells, and explain Adelson and Movshon's two-stage hypothesis neurophysiologically. The intersection-of-constraint-lines solution of the hypothesis is equivalent to the inverse Hough transform processed in motion-detection cells. We propose tests for validating this cell model using microelectrodes and optical imaging.

Cell model Image-motion detection Hough transform Spatio-temporal correlation Magnocellular pathway

1. INTRODUCTION

The perception of visual motion serves many roles, including depth perception by motion parallax and the control of eye movements. By integrating local image motion, i.e. the two-dimensional (2-D) motion in each small region of the visual field, the perception process is performed.

Adelson and Movshon (1982) proposed that the human visual system determines the 2-D motion of a stimulus in two stages. First, the visual system measures the one-dimensional (1-D) velocities perpendicular to oriented components, such as lines and edges, within the stimulus. Then, it combines these velocities for the 2-D motion detection.

This two-stage hypothesis was initially supported by a psychophysical observation. Using a moving-plaid pattern (the sum of two differently oriented moving gratings), Adelson and Movshon (1982) confirmed that the 2-D motion of the plaid pattern is perceived through its decomposition into 1-D velocities. Welch (1989) found that speed discrimination for moving-plaid stimuli is consistent with this hypothesis. Although the recombination rule of the hypothesis, which is based on the intersection-of-constraint-lines (IOC) solution, was challenged (Ferrera & Wilson, 1990; Rubin & Hochstein, 1993), psychophysical observations have recently confirmed the rule's consistency (Burke & Wenderoth, 1993).

Movshon, Adelson, Gizzi and Newsome (1985) found electrophysiological support for this hypothesis. They discovered two types of cell in the visual cortex of monkeys: component-motion selective cells (Component cells) and pattern-motion selective cells (Pattern cells). Component cells respond best to a moving-plaid pattern when the axis of motion of one of the component gratings coincides with the cell's preferred axis of motion. Pattern cells respond best when the axis of motion of the plaid pattern itself coincides with the cell's preferred axis of motion. Component cells, found both in the primary visual cortex (V1) and in the middle temporal area (MT), analyze the 1-D velocities of component gratings. Pattern cells in area MT detect the 2-D motion of a plaid pattern. Rodman and Albright (1989) confirmed the presence of these cell types in the MT area of monkeys. Their work clarified a correspondence between the cell types and the type I and II cells that were initially distinguished by Albright (1984).

The various models based on this two-stage hypothesis can be divided into two classes: those using the spatio-temporal scheme, and those using an inverse Hough transform.

*Fujitsu Laboratories Ltd, 1015 Kamikodanaka, Nakahara-ku, Kawasaki 211, Japan

†To whom all correspondence should be addressed. [*Fax* 81 44 754 2582].

For the first stage, Heeger (1987) and Grzywacz and Yuille (1990) used spatio-temporal energy filters (Adelson & Bergen, 1985) to measure motion energies corresponding to the 1-D velocities. For the second stage, they combined the energies in the spatio-temporal frequency domain to detect the 2-D motion of moving stimuli. Watson and Ahumada (1985) used scalar motion sensors in the frequency domain, then in the second stage, they used vector motion sensors to combine the scalar sensors' output and detect 2-D motion.

In contrast, using an inverse Hough transform, Sereno (1986, 1987, 1993) implemented the second stage as a neural network linking the V1 and MT cells. Sereno did not give an algorithm for the first stage. Fennema and Thompson (1979) used the gradient scheme (Limb & Murphy, 1975) to measure the 1-D velocities, then combined the velocities using the transform to detect 2-D motion. Ogata and Sato (1991) used the transform to combine the scalar-motion-sensors' output and detect the 2-D motion.

These models, however, involve some processing steps that cannot be implemented by neurons easily: the Gabor-function-type oriented filters and the square of the filter's output (Heeger, 1987; Grzywacz & Yuille, 1990), the division used in the gradient scheme (Fennema & Thompson, 1979), and the Fourier transform (Watson & Ahumada, 1985; Ogata & Sato, 1991).

We found that five types of cell on the magnocellular pathway of the visual cortex constitute a function hierarchy for detecting 2-D motion. Using Hough and inverse Hough transforms and Reichardt's spatio-temporal correlation, we modeled the cell types as a series of formulas that represent three types of synaptic functions in neurons: the postsynaptic excitation and inhibition; the synaptic transmission efficiency; and a multiplication-like function. The modeled cells explain the two-stage hypothesis (Adelson & Movshon, 1982) neurophysiologically. They detect 2-D motion from a variety of moving stimuli, including dots, straight lines, curves, edges, and plaid patterns.

Some parts of the material in this paper—the method for detecting 2-D motion, the correspondence between the modeled cells and the cells on the magnocellular pathway, and some computer simulations—have been presented previously (Kawakami, Okamoto & Morita, 1992; Kawakami & Okamoto, 1992, 1993, 1995; Okamoto, Kawakami & Oka, 1994).

2. CELL MODEL

2.1. Visual Pathway

This section proposes a visual pathway for detecting 2-D motion, and describes the neurophysiological properties of cells on the pathway. (Note that data from cats and monkeys are suffixed by $^{+}$ and $^{++}$, respectively.)

The anatomical structure of the magnocellular pathway in monkeys, which processes image motion and stereo disparity, has been studied extensively (Hubel & Livingstone, 1987; Zeki & Shipp, 1988; Livingstone & Hubel, 1988; Maunsell, Nealey & DePriest, 1990; Merigan & Maunsell, 1993; Nealey & Maunsell, 1994; Casagrande, 1994). The pathway begins with Y-like retinal ganglion cells (Leventhal, Rodieck & Dreher, 1981; Perry, Oehler & Cowey, 1984), then passes through the magnocellular layers of the lateral geniculate nucleus (LGN) to layer 4Cα of area V1 (Hubel & Wiesel, 1972; Boothe, Greenough, Lund & Wrege, 1979). Layer 4Cα has strong connections with layer 4B of V1 (Lund & Boothe, 1975; Fitzpatrick, Lund & Blasdel, 1985), which sends a direct projection to MT (Lund, Lund, Hendrickson, Bunt & Fuchs, 1976; Spatz, 1977; Maunsell & Van Essen, 1983b).

Based on the presence of lagged and nonlagged LGN cells, we propose a visual pathway for detecting 2-D motion (Fig. 1). The pathway is obtained by inserting a lagged cell branch into the magnocellular pathway. The layer 4Cα cells and nondirectionally selective (NDS) simple cells in the lagged branch have not yet been validated neurophysiologically. The following sections show that five types of cell on this pathway, excluding layer 4 Cα cells, constitute a function hierarchy for motion detection.

The neurophysiological properties of each cell type on the pathway are as follows.

The population of LGN cells in cats is divided into two classes, i.e. lagged and nonlagged LGN cells

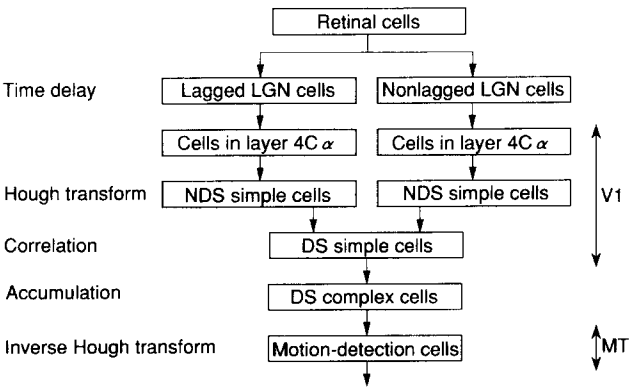

FIGURE 1. Proposed visual pathway for detecting 2-D motion from a moving stimulus. The pathway is obtained by inserting a lagged cell branch—composed of lagged LGN cells, layer 4Cα cells, and NDS simple cells—into the magnocellular visual pathway. DS complex cells are present in both areas V1 and MT. We also propose that the five types of cell on this pathway constitute a function hierarchy, shown on the left, for 2-D motion detection. (1) Lagged LGN cells with a fixed time delay t_d and nonlagged cells divide a retinal image into a lagged image and a nonlagged image of LGN cells. Based on the spatial displacement between the two images, 1-D velocities of oriented components can be determined. (2) Cells in layer 4Cα of area V1 act as a relay. (3) NDS simple cells perform a Hough transform, through which each oriented component is converted to the activation of an NDS simple cell. The position of this cell corresponds to the component's location and orientation. (4) DS simple cells perform a spatio-temporal correlation between the lagged and nonlagged NDS simple cells to detect the components' 1-D velocities. (5) Accumulating the DS simple cell responses, a group of DS complex cells along a sine wave fire over the cell array. The amplitude and phase of the wave correspond to the motion's speed and direction. (6) Finally, to extract the wave of activated complex cells, motion-detection cells in area MT perform an inverse Hough transform.

(Mastronarde, 1987a; Humphrey & Weller, 1988; Saul & Humphrey, 1990). The lagged cell class has a longer temporal-latency t_d to the visual response than the nonlagged cell class. Both lagged and nonlagged LGN cells have the same spatial properties, such as concentric receptive fields of the same size. These two classes were initially reported for X-cells (Mastronarde, 1987a; Humphrey & Weller, 1988) belonging to the parvocellular visual pathway, then reported for Y-cells (Saul & Humphrey, 1990) belonging to the magnocellular pathway. Mastronarde (1987b$^+$) and Hartveit and Heggelund (1993$^+$) clarified the physiological process by which this latency is produced in the lagged LGN cells.

Cells in layer 4Cα of area V1, which act as a relay, have concentric receptive fields similar to those in the retinal and LGN cells (Enroth-Cugell & Robson, 1966$^+$; Hubel & Wiesel, 1961$^+$, 1977^{++}).

NDS and directionally selective (DS) simple cells are present in layers 4B and 6 of area V1 (Hubel & Wiesel, 1968^{++}; Henry, Harvey & Lund, 1979$^+$; Gilbert & Wiesel, 1981$^+$; Ferster & Lindström, 1983$^+$; Maunsell & Newsome, 1987^{++}). DS complex cells, which correspond to the Component and type I cells (Section 4.2), are present both in layers 2, 3, and 5 of area V1 (Gilbert & Wiesel, 1981$^+$; Ferster & Lindström, 1983$^+$; Movshon *et al.*, 1985^{++}; Edelstyn & Hammond, 1988$^+$) and in layers 4 and 6 of area MT (Movshon *et al.*, 1985^{++}).

Motion-detection cells, which correspond to the Pattern and type II cells (Section 4.2), are present in layers 2, 3, and 5 of area MT of monkeys (Movshon *et al.*, 1985). The cells respond selectively to the local 2-D motion of single and random dots and plaid patterns (Albright, 1984^{++}; Movshon *et al.*, 1985^{++}; Tanaka, Hikosaka, Saito, Yukie, Fukada & Iwai, 1986^{++}; Rodman & Albright, 1987^{++}, 1989^{++}; Malonek, Tootell & Grinvald, 1992^{++}), independent of the location, orientation, and contrast polarity of these stimuli. About a quarter of MT cells in monkeys are Pattern cells and about one half are Component cells (Movshon *et al.*, 1985).

Responses of these five cell types to traditionally used bar stimuli are summarized in Table 1. The contrast polarity is defined by whether the stimulus is brighter than the background or not. The bar stimulus moves perpendicular to its orientation.

Cells in the medial superior temporal area (MST) of monkeys integrate the local 2-D motions (detected by the MT cells) over the MST cells' large receptive fields, then detect higher order motion features, e.g. rotation, dilation, and contraction (Saito *et al.*, 1986; Tanaka & Saito, 1989; Duffy & Wurtz, 1991a,b; Saito, 1993).

TABLE 1. Selectivities of cell responses to bar stimulus parameters

	Bar stimulus parameters			
Type	Location	Orientation	1-D velocity	Contrast polarity
LGN[1]	○	×	×	○
NDS simple[2]	○	○	×	○
DS simple[3]	○	○	○	×
DS complex[4]	×	○	○	×
Motion detection[5]	×	○	○	×

○, Selective; ×, not selective. Note: Data for cats and monkeys are suffixed with $^+$ and $^{++}$, respectively.

[1]Hubel and Wiesel (1961$^+$, 1977^{++}).

[2]Hubel and Wiesel (1959$^+$, 1962$^+$); Schiller, Finlay and Volman (1976^{++}).

[3]Hubel and Wiesel (1959$^+$, 1962$^+$); Schiller *et al.* (1976^{++}); Henry (1977$^+$); Maske, Yamane and Bishop (1985$^+$); Yamane, Maske and Bishop (1985$^+$); Baker (1988$^+$); these are B cells (Maske *et al.*, 1985$^+$) responding independently of a bar's contrast polarity.

[4]Hubel and Wiesel (1962$^+$); Schiller *et al.* (1976^{++}); Henry (1977$^+$); Maske *et al.* (1985$^+$); Baker (1988$^+$); Albright (1984^{++}); Rodman and Albright (1987^{++}, 1989^{++}).

[5]Maunsell and Van Essen (1983a^{++}); Albright (1984^{++}); Mikami *et al.* (1986a^{++}); Rodman and Albright (1987^{++}, 1989^{++}); Snowden *et al.* (1992^{++}); Lagae, Raiguel and Orban (1993^{++}).

2.2. Detecting 1-D Velocity

This section shows that LGN cells and NDS and DS simple cells constitute a function hierarchy for detecting the 1-D velocity of a moving line: time delay, Hough transform, and a spatio-temporal correlation. Figure 2 outlines our 1-D velocity detection process.

2.2.1. Time delay in LGN cells

Figure 2A and B shows that a line moving across the retinal cell array is converted to two parallel lines moving across the lagged and nonlagged LGN cell arrays. The spatial displacement between the lines Δd equals the product of the line's 1-D velocity V_{1D} and the fixed time delay t_d of the lagged LGN cells. Hence, the Δd displacement can determine the V_{1D} velocity:

$$V_{1D} = \Delta d / t_d. \tag{1}$$

The two LGN cell types transform a spatio-temporal parameter (the V_{1D} velocity) into a spatial parameter (the Δd displacement). This transform enables the neuronal networks, where spatial processing is executed, to measure the 1-D velocity.

The responses of lagged and nonlagged LGN cells are modeled as a convolution operation (Marr & Hildreth, 1980) between retinal cell responses $I(x, y, t)$ and a function DOG(u, v):

$$_{L}\mathrm{LGN}(x, y) = \sum_u \sum_v I(x-u, y-v, t-t_d)\,\mathrm{DOG}(u, v) \tag{2}$$

$$_{NL}\mathrm{LGN}(x, y) = \sum_u \sum_v I(x-u, y-v, t)\,\mathrm{DOG}(u, v);$$

x and y are LGN cell addresses, and t is time. u and v are summed over all retinal cells in the receptive field of each LGN cell. The DOG(u, v) function, which represents a pair of excitatory and inhibitory concentric receptive fields in an LGN cell, is given by

$$\mathrm{DOG}(u, v) = \exp[-(u^2 + v^2)/s^2] - 0.326\exp[-(u^2 + v^2)/(1.75s)^2]. \tag{3}$$

We obtained equation (3) by converting the 1-D

observation (Wilson, 1978) into a 2-D form; s is the degree of broadness. The convolution operation differentiates and enhances retinal cell images.

2.2.2. *Hough transform in NDS simple cells*

We propose that NDS simple cells perform a Hough transform (Hough, 1962). Figure 2C shows that, through the transform, the parallel lines in the nonlagged and lagged LGN cell arrays are converted to two NDS simple cells activated at (ρ_0, θ_0) and (ρ_1, θ_0) with the same θ_0 orientation. This transform enables the Δd displacement between the lines to be measured one-dimensionally as the difference between the cells' ρ coordinates, i.e. $\rho_0 - \rho_1$.

We model the responses of NDS simple cells in the lagged and nonlagged branches as the Hough transformation of the LGN cell responses (Appendix A.1):

$$_{L}SC_{NDS}(\rho, \theta) = \sum_{x} \sum_{y} {}_{L}LGN(x, y)\, \delta(\rho - x\cos\theta - y\sin\theta) \quad (4)$$

$$_{NL}SC_{NDS}(\rho, \theta) = \sum_{x} \sum_{y} {}_{NL}LGN(x, y)\, \delta(\rho - x\cos\theta - y\sin\theta);$$

ρ and θ are NDS simple cell addresses; x and y are summed over all LGN cells within a rectangular receptive field that corresponds to the θ coordinate of each NDS simple cell [Fig. A2(ii) in Appendix A]. We assume that these cells are arranged two-dimensionally in layer 4B of area V1 as the (ρ, θ) array (Section 6.1).

Based on the property that the delta function $\delta(\zeta) = 1$ for $\zeta = 0$ and $\delta(\zeta) = 0$ for $\zeta \neq 0$, equation (4) indicates that an NDS simple cell at (ρ, θ) fires after accumulating the responses of a group of LGN cells along a straight line $\rho - x\cos\theta - y\sin\theta = 0$ in the (x, y) LGN cell array. Thus, the simple cell detects a line with ρ location and θ orientation. The isolated firing to the line represents the cell's location and orientation selectivities; the cell responds based on the line's contrast polarity.

The Hough transform was initially presented as an image-processing method for detecting lines in noisy pictures (Hough, 1962; Duda & Hart, 1972, 1973; Ballard & Brown, 1982). Then, its application to neurophysiology was suggested (Barlow, 1980; Ballard, Hinton & Sejnowski, 1983; Blasdel, 1992b; Obermayer & Blasdel, 1993; Blasdel & Obermayer, 1994). However, to our knowledge, the transform has not been used to model actual cell responses. Using Radon transform, Okajima (1986) modeled the nonlagged NDS simple cell responses as an equation equivalent to equation (4).

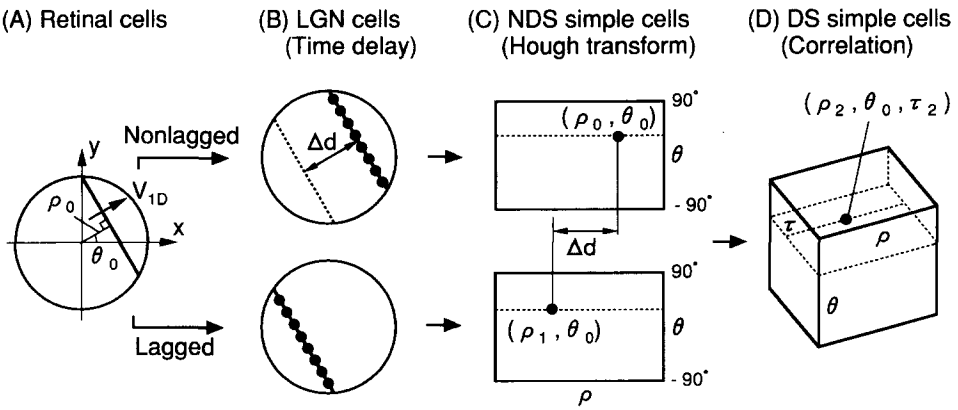

FIGURE 2. Proposed function hierarchy for detecting the 1-D velocity of a moving line. The hierarchy is composed of a time delay generated by lagged LGN cells (B), Hough transform processed in NDS simple cells (C), and a spatio-temporal correlation processed in DS simple cells (D). Each cell is arranged in the orthogonal arrays; retinal cells and LGN cells in the (x, y) arrays, NDS simple cells in the (ρ, θ) array, and DS simple cells in the (ρ, θ, τ) array. (Filled circles in the arrays are activated cells.) (A) We assume a line moving with ρ_0 location, θ_0 orientation, and a 1-D velocity of V_{1D} speed and θ_0 direction. The ρ_0 location is the perpendicular distance from the origin to the line, and the line moves perpendicular to its orientation. The line's movement direction is represented by the same variable θ_0 as its orientation. (B) The line is converted to two parallel lines composed of activated LGN cells in the lagged and nonlagged arrays. These lines move with the spatial displacement between them Δd proportional to the V_{1D} velocity. This displacement can determine the line's V_{1D} velocity as $\Delta d/t_d$, based on the fixed time delay t_d of lagged LGN cells. (To show the Δd displacement explicitly, the dotted line in the nonlagged array represents the line in the lagged array.) (C) The Hough transform [Fig. A1(i) in Appendix A] converts these parallel lines into two NDS simple cells activated at (ρ_0, θ_0) and (ρ_1, θ_0) with the same θ_0 orientation, where $\rho_1 = \rho_0 - \Delta d = \rho_0 - V_{1D}t_d$. The cell's coordinates coincide with the ρ location and θ orientation of the line in each LGN cell array. Thus, the displacement above is transformed into the Δd difference between the cells' ρ coordinates. The position of such a cell moves along the ρ coordinate, with the V_{1D} velocity. The NDS simple cell is connected with all LGN cells on the corresponding line (●). (D) A DS simple cell at $(\rho_2, \theta_0, \tau_2)$, which is connected with the lagged and nonlagged NDS simple cells at (ρ_0, θ_0) and (ρ_1, θ_0), performs a spatio-temporal correlation between the cells' responses to detect the 1-D velocity of the line. The DS cell will respond if a line, which has the θ_0 orientation and a V_{1D} 1-D velocity equal to the Δd difference divided by the t_d time delay, crosses its receptive field. Under such conditions, activation from the two NDS simple cells coincides (i.e. is correlated) to cause activation in the DS simple cell. Hence, this DS simple cell detects the line's 1-D velocity as $\Delta d/t_d$. The position of such a cell moves along the ρ coordinate, with the V_{1D} velocity. Text details this detection and shows that the moving line causes activation in a DS simple cell at $((\rho_0 + \rho_1)/2, \theta_0, V_{1D}t_d/2)$.

2.2.3. Spatio-temporal correlation in DS simple cells

We propose that DS simple cells perform a spatio-temporal correlation to detect the 1-D velocity of the line. Figure 2D shows that, executing the correlation between the two NDS simple cells above, a DS simple cell detects the line's V_{1D} velocity as $\Delta d/t_d$.

Introducing a variable τ, we model the response of a DS simple cell as the cross-correlation between the responses of lagged and nonlagged NDS simple cells whose ρ coordinates are shifted symmetrically by $\pm\tau$:

$$SC_{DS}(\rho, \theta, \tau) = {}_{L}SC_{NDS}(\rho - \tau, \theta)\ {}_{NL}SC_{NDS}(\rho + \tau, \theta); \quad (5)$$

ρ, θ, and τ are DS simple cell addresses. We assume that these cells are arranged three-dimensionally in layer 4B of area V1 as a horizontal (ρ, θ) array with a depth arrangement of τ (Section 6.1). This spatio-temporal correlation, containing the τ spatial shift and the t_d fixed time delay, is an application of Reichardt's correlation-type movement detector to the ρ coordinate of the Hough plane. The detector was initially proposed for a fly's visual system (Reichardt, 1961, 1987; Barlow & Levick, 1965; Van Santen & Sperling, 1984, 1985; Hildreth & Koch, 1987; Borst & Egelhaaf, 1989; Egelhaaf & Borst, 1993).

Based on equation (5), a detailed description of the 1-D velocity detection is presented: the response of a DS simple cell at $(\rho_2, \theta_0, \tau_2)$ is discussed. The cell is connected with the spatially-shifted lagged and nonlagged NDS simple cells at (ρ_1, θ_0) and (ρ_0, θ_0), where $\rho_1 = \rho_0 - \Delta d = \rho_0 - V_{1D}t_d$ (Fig. 2C and D). The DS cell will fire if activations of these NDS simple cells [the first and second terms in equation (5)] coincide. This occurs when the cell's ρ_2 and τ_2 coordinates satisfy the relationship, $\rho_2 = (\rho_0 + \rho_1)/2$ and $\tau_2 = V_{1D}t_d/2$, which results from the coincidence condition, i.e. $\rho_2 - \tau_2 = \rho_1$ and $\rho_2 + \tau_2 = \rho_0$. Based on this τ_2 coordinate, the 1-D velocity of the line is determined by

$$V_{1D} = 2\tau_2/t_d. \quad (6)$$

Consequently, the moving line causes activation in a DS simple cell at $((\rho_0 + \rho_1)/2, \theta_0, V_{1D}t_d/2)$.

Therefore, equation (5) indicates that a DS simple cell at (ρ, θ, τ) fires to detect a line with $\rho + \tau$ location, θ orientation, and $2\tau/t_d$ 1-D velocity, independent of the line's contrast polarity. The isolated firing to the line represents the cell's location, orientation, and 1-D velocity selectivities. We note that DS simple cells with different τ coordinates have different Δd selectivities, and hence different V_{1D} selectivities. (To simplify the description, τ also denotes the V_{1D} velocity, eliminating the coefficient $t_d/2$.)

We note that a band-pass filtering by the DOG(u, v) function of LGN cells [equation (3)] prevents the spatial aliasing (Van Santen & Sperling, 1984, 1985; Borst & Egelhaaf, 1989) that corrupts this spatio-temporal correlation.

2.3. Detecting 2-D Motion

This section shows that DS complex cells and motion-detection cells constitute a function hierarchy for detecting 2-D motion of moving lines by combining their 1-D velocities: an accumulation and an inverse Hough transform.

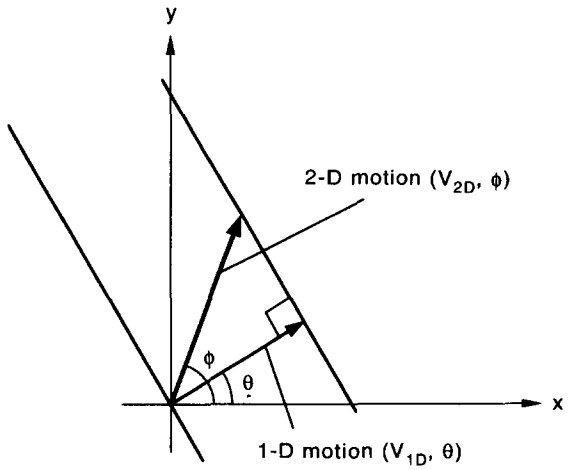

FIGURE 3. The 1-D velocity of a line (V_{1D} speed and θ direction) is the orthogonal projection of its 2-D motion (V_{2D} speed and ϕ direction) in the direction perpendicular to it. Three forms of this relationship are expressed in equation (7).

This combination of 1-D velocities is executed based on the following relationship between the 1-D velocity (V_{1D}, θ) and the 2-D motion (V_{2D}, ϕ) of a line (Fig. 3):

$$\begin{aligned} V_{1D} &= \mathbf{V_{2D}u} \\ &= V_{2D}\cos(\phi - \theta) \\ &= V_x\cos\theta + V_y\sin\theta, \end{aligned} \quad (7)$$

where

$$\begin{aligned} \mathbf{V_{2D}} &= (V_x, V_y) \\ &= V_{2D}(\cos\phi, \sin\phi) \end{aligned} \quad (8)$$

and

$$\mathbf{u} = (\cos\theta, \sin\theta). \quad (9)$$

V_{1D}, θ, and $\mathbf{u}$ are the speed, direction, and unit vector of the 1-D velocity. V_{2D}, ϕ, V_x, and V_y are the speed, direction, and Cartesian coordinates of 2-D motion. Equation (7) represents a constraint line (Adelson & Movshon, 1982; Ferrera & Wilson, 1990) in the (V_x, V_y) velocity space. This line indicates all 2-D motions that can exist in a line moving with the (V_{1D}, θ) 1-D velocity.

Adelson and Movshon (1982) presented the IOC solution (Fig. 4). We show that the inverse Hough transform processed in motion-detection cells executes this solution, following the 1-D velocity detection by DS complex cells. Figure 5 outlines our 2-D motion detection process.

2.3.1. Accumulation in DS complex cells

We propose that a DS complex cell accumulates the responses of all DS simple cells with the same θ orientation and τ 1-D velocity selectivities but different ρ location selectivity. Figure 5A–C shows that, through this accumulation, the (V_x, V_y) 2-D motion of the moving

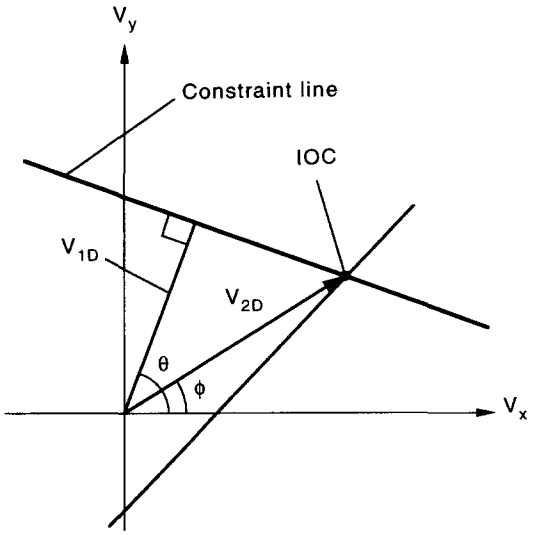

FIGURE 4. The IOC solution (Adelson & Movshon, 1982) for measuring the (V_{2D}, ϕ) 2-D motion of moving lines. The V_{1D} speed and θ direction of a component line give the foot and angle of a constraint line [equation (7)] in the (V_x, V_y) velocity space. Then, the 2-D motion is measured at the intersection (V_{2D}, ϕ) of such constraint lines.

lines is converted into a sine wave composed of activated DS complex cells over the (θ, τ) cell array. The sine wave is expressed by

$$\tau = \tau_x \cos\theta + \tau_y \sin\theta, \tag{10}$$

where τ_x and τ_y are defined as follows:

$$\tau_x = (t_d/2)V_x \tag{11}$$

$$\tau_y = (t_d/2)V_y.$$

This wave is a representation of the constraint line [equation (7)] in the (θ, τ) array, which was obtained by inserting equation (6) into the third form of equation (7).

The τ_3 amplitude and θ_3 phase of the wave correspond to the 2-D motion's V_{2D} speed and ϕ direction, with the relationship of $V_{2D} = 2\tau_3/t_d$ and $\phi = \theta_3$. Hence, we can detect the 2-D motion by measuring this wave.

We model the response of a DS complex cell as the accumulation of the DS complex cell responses along the ρ coordinate.

$$CC_{DS}(\theta, \tau) = \sum_{\rho} SC_{DS}(\rho, \theta, \tau); \tag{12}$$

θ and τ are DS complex cell addresses. We assume that these cells are arranged two-dimensionally as the (θ, τ) array in areas V1 and MT, as presented previously (Sereno, 1993; Rodman & Albright, 1989). Equation (12) indicates that a DS complex cell at (θ, τ) fires to detect a line with θ orientation and τ 1-D velocity, independent of the line's ρ location and contrast polarity. The isolated firing to the line represents the cell's orientation and 1-D velocity selectivities.

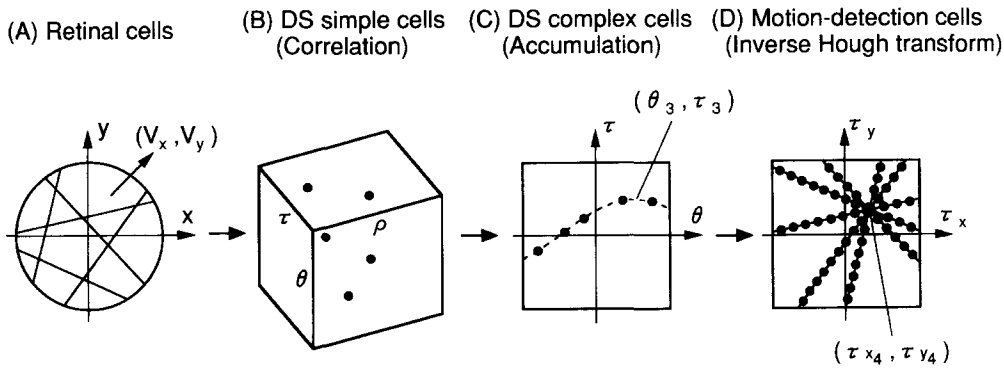

FIGURE 5. Proposed function hierarchy for detecting the 2-D motion of moving lines. The hierarchy is composed of an accumulation processed in DS complex cells (C) and an inverse Hough transform processed in motion-detection cells (D), following the hierarchy for the 1-D velocity detection (Fig. 2B–D). (A) We assume lines moving with (V_x, V_y) 2-D motion. (B) The preceding hierarchy converts the lines into activated DS simple cells in the (ρ, θ, τ) array; the cells' coordinates correspond to the lines' ρ locations, θ orientations, and V_{1D} velocities. (C) Accumulating the DS simple cell responses along the ρ coordinate, a group of DS complex cells along a sine wave [equation (10)] fire over the (θ, τ) array. The wave indicates all (V_{1D}, θ) 1-D velocities that can exist in a stimulus moving with the 2-D motion. The τ_3 amplitude and θ_3 phase of the wave correspond to the 2-D motion's speed and direction, with the relationship of $\tau_3 = (t_d/2)\sqrt{(V_x^2 + V_y^2)}$ and $\theta_3 = \tan^{-1}(V_y/V_x)$. Hence, the lines' 2-D motion is converted to this sine wave. A DS complex cell is connected to all DS simple cells with the same θ orientation and τ 1-D velocity selectivities. (D) Motion-detection cells perform the inverse Hough transform to extract the sine wave [Fig. A1(ii) in Appendix A]. The transform converts the complex cells' responses on the wave into a group of lines composed of activated motion-detection cells. These lines intersect at a point (τ_{x4}, τ_{y4}) corresponding to the wave's (θ_3, τ_3) peak and proportional to the 2-D motion. This is expressed as $(\tau_{x4}, \tau_{y4}) = \tau_3(\cos\theta_3, \sin\theta_3) = (t_d/2)(V_x, V_y)$. Hence, this transform extracts the sine wave as the intersection point. It causes most intensive activation in a motion-detection cell at the $(t_d/2)(V_x, V_y)$ point. From the cell's coordinates, the 2-D motion is determined. This motion-detection cell is connected with all DS complex cells on the sine wave over the (θ, τ) array. Consequently, the sequential processing by the five cell types (Figs 2B–D and 5C and D) converts the lines' 2-D motion into the activation of a motion-detection cell at the $(t_d/2)(V_x, V_y)$ point. This processing also converts each component line in the (x, y) retinal cell array into a line, in the (τ_x, τ_y) array, that is parallel to the line in the (x, y) array and passes through the point. This line in the (τ_x, τ_y) array corresponds to a constraint line given by the (V_{1D}, θ) 1-D velocity of the line (Section 5.1).

2.3.2. Inverse Hough transform in motion-detection cells

We propose that motion-detection cells perform an inverse Hough transform to extract the sine wave for 2-D motion detection. Figure 5D shows that the transform extracts the wave as the (τ_{x4}, τ_{y4}) intersection of lines composed of activated motion-detection cells, with the relationship of $(\tau_{x4}, \tau_{y4}) = (t_d/2)(V_x, V_y)$. By inserting the point's coordinates into equation (11), the 2-D motion of the lines is given by

$$\mathbf{V}_{2D} = (2/t_d)(\tau_{x4}, \tau_{y4}). \quad (13)$$

This inverse Hough transform computation is equivalent to the IOC solution, because the lines above correspond to constraint lines (Section 5.1).

We model the response of a motion-detection cell as the inverse Hough transformation of the DS complex cell responses (Appendix A.2):

$$\mathrm{MDC}(\tau_x, \tau_y) = \sum_{\theta} \sum_{\tau} \mathrm{CC}_{DS}(\theta, \tau)\, \delta(\tau - \tau_x \cos\theta - \tau_y \sin\theta); \quad (14)$$

τ_x and τ_y are motion-detection cell addresses, and θ and τ are summed over all cells in the DS complex cell array. We assume that these cells are arranged two-dimensionally in area MT as the (τ_x, τ_y) array which is equivalent to the (V_x, V_y) velocity space (Section 5.1).

Based on the $\delta(\zeta)$ definition above, equation (14) indicates that a motion-detection cell at (τ_x, τ_y) fires after accumulating the responses of a group of DS complex cells along a sine wave, $\tau - \tau_x \cos\theta - \tau_y \sin\theta = 0$, in the (θ, τ) array. Hence, this cell extracts the sine wave with $\sqrt{(\tau_x^2 + \tau_y^2)}$ amplitude and $\tan^{-1}(\tau_y/\tau_x)$ phase.

In summary, our cell sequence detects 2-D motion from moving stimuli, as follows. LGN cells, NDS and DS simple cells, and DS complex cells convert the lines' (V_x, V_y) 2-D motion into a sine wave composed of activated DS complex cells, $\tau - (t_d V_x/2)\cos\theta - (t_d V_y/2)\sin\theta = 0$, over the (θ, τ) array. Extracting this wave, a motion-detection cell at $(t_d/2)(V_x, V_y)$ fires. From this cell's coordinates, the 2-D motion is determined.

We note that x, y, u, v, ρ, θ, τ, τ_x, and τ_y in equations (2–6) and equations (10–14) are integers representing cell addresses. The addresses must be multiplied by the interval between adjacent retinal cells. To simplify the description, we have eliminated this coefficient.

2.4. Representation in Neuronal Network

In this section, we propose that the series of formulas [equations (2, 4, 5, 12, and 14)] represents the neuronal network linking retinal cells and motion-detection cells.

First, we show that three operations used in the formulas can be implemented by synaptic functions of neurons. The first is addition and subtraction, which are implemented by the postsynaptic excitation and inhibition (Kuffler, Nicholls & Martin, 1984). Equations (2, 4, 12, and 14) use this operation as the accumulation. The second operation is multiplication with constant coefficients, which is implemented by the synaptic transmission efficiency (Kuffler *et al.*, 1984). Equation (2) uses this operation as the multiplication of retinal cell responses with the DOG(u, v) constant coefficients. The third operation is a multiplication-like function, which is assumed to be a characteristic of certain synapses (Torre & Poggio, 1978; Van Santen & Sperling, 1985; Hildreth & Koch, 1987; Schmid & Bulthoff, 1988; Borst & Egelhaaf, 1989; Egelhaaf & Borst, 1993). Equation (5) uses this operation. Hence, all the modeled cells are described by synaptic functions of neurons.

Based on these synaptic functions, we propose that the series of formulas represents the neuronal connections in the cell sequence as follows: (1) each LGN cell is connected with all retinal cells in its concentric receptive field [equation (3)] through the synaptic transmission efficiency; (2) each layer 4Cα cell is connected with an LGN cell; (3) each NDS simple cell is connected with all 4Cα cells on a line segment within the rectangular receptive field [Fig. A2(iii) in Appendix A]; (4) each DS simple cell is connected to a pair of lagged and nonlagged NDS simple cells with the same orientation selectivity. Multiplying these cell-pair responses, the DS cell fires; (5) each DS complex cell is connected to all DS simple cells with the same orientation and 1-D velocity selectivities but different location selectivity; and, finally, (6) each motion-detection cell is connected with all DS complex cells on a sine wave [equation (10)].

This is, to our knowledge, the first model of the neuronal network linking retinal cells and motion-detection cells in area MT as a sequence of formulas that represent the synaptic functions of neurons.

3. SIMULATION RESULTS

The computer simulations show that the modeled cell sequence [equations (2, 4, 5, 12, 14)], formulated using 2.6×10^5 connections in a receptive field (Appendix B), correctly detects 2-D motion from a variety of moving stimuli (Figs 6–8).

3.1. Straight Lines

Using one of the simplest 2-D motion stimuli (i.e. a cross inclined by 20 deg), we showed how the cell sequence detects 2-D motion (Fig. 6A).

LGN cells enhance the retinal cell images. Then, a sharpened cross appears surrounded by inhibitory responses [Fig. 6A(i)].

Figure 6A(ii–iv) shows that the three types of modeled cell correctly measure the line's parameters (i.e. ρ location, θ orientation, and τ 1-D velocity), based on the cell coordinates. In each NDS simple cell array, the coordinates of two cells coincide with the ρ location and θ orientation of the bars of the cross. These cells fire to detect the bars. In the DS simple cell array showing the cross-sectional response at $\theta = 20$ deg, a cell whose coordinates coincide with the $\theta(=20$ deg) orientation and τ 1-D velocity of one of the bars fires to detect it; the cell fires with the ρ coordinate of $(\rho_0 + \rho_1)/2$ shown in the legend to Fig. 2D. In the DS complex cell array, two cells

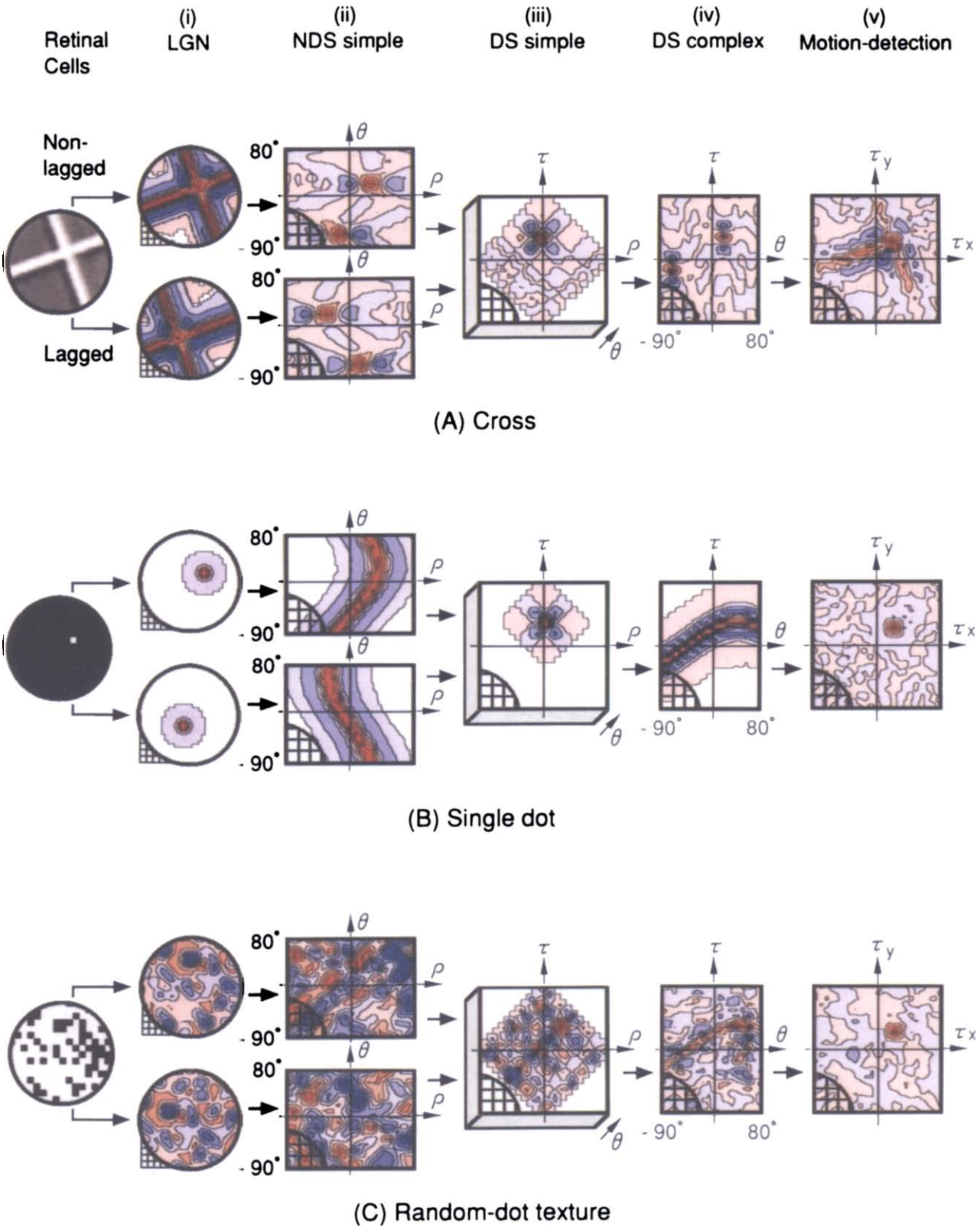

FIGURE 6. Sequential processing by the modeled cells to detect 2-D motion from (A) a moving cross, (B) a single dot, and (C) a random-dot texture. Cells are arranged in the orthogonal array of each cell type (Figs 2 and 5), and the array size is shown in Appendix B. Each lattice point in the lower left corner of an array corresponds to 2 × 2 cells. The normalized firing intensity at each cell is calculated using equations (2, 4, 5, 12, and 14), then, with the exception of retinal cells, depicted in a contour map. Excitatory responses are in red, and inhibitory ones in blue. Each stimulus moved towards the upper right with ($V_x = 6/t_d$, $V_y = 6/t_d$) 2-D motion. The stimulus caused the most intensive activation in a motion-detection cell at ($t_d/2$)(V_x, V_y), i.e. at (3, 3). From this cell's coordinates, the stimulus' 2-D motion was determined correctly.

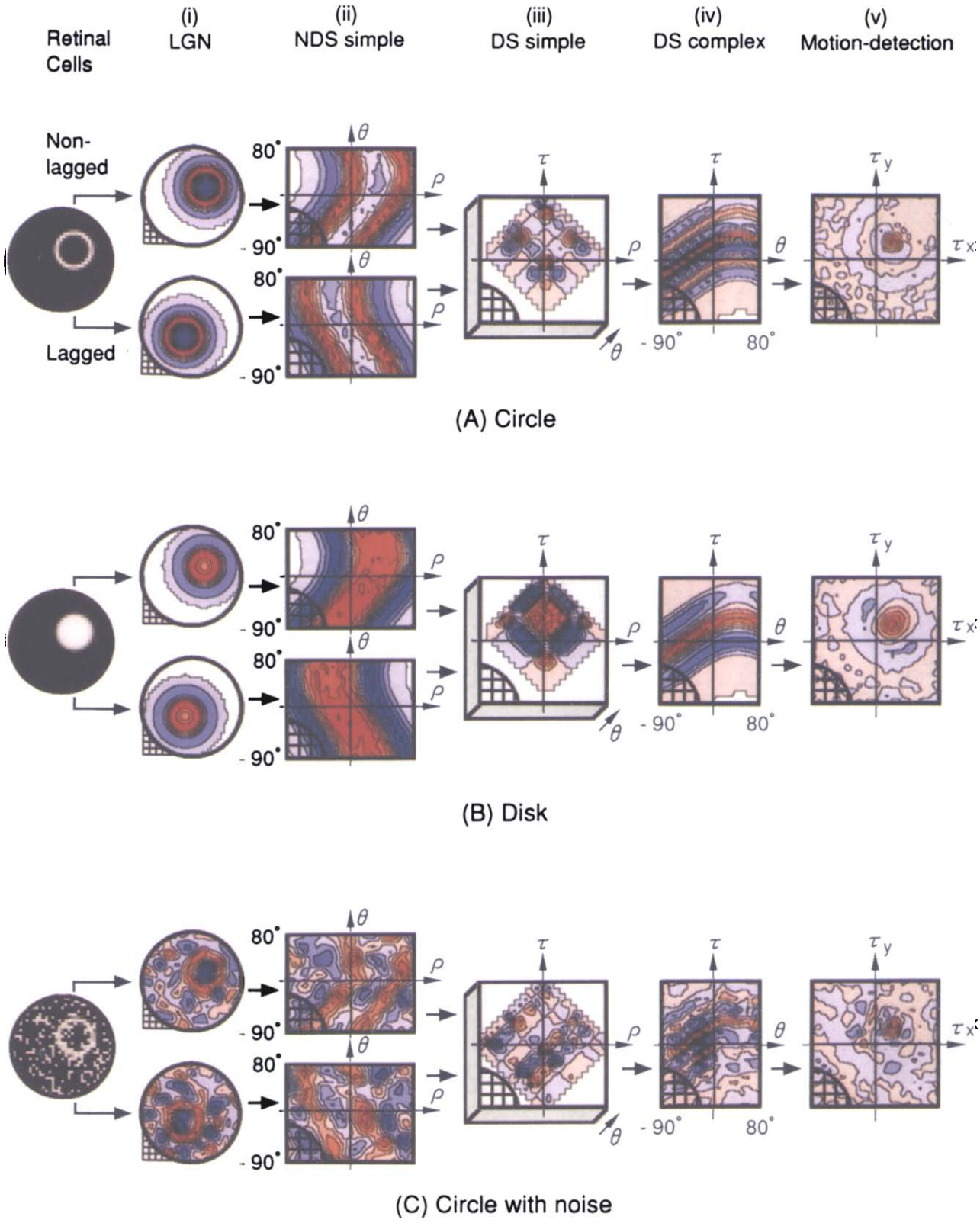

FIGURE 7. Sequential processing by the modeled cells to detect 2-D motion from (A) a moving circle, (B) a disk, and (C) a circle with noise. Descriptions such as the 2-D motion of each stimulus are the same as in Fig. 6.

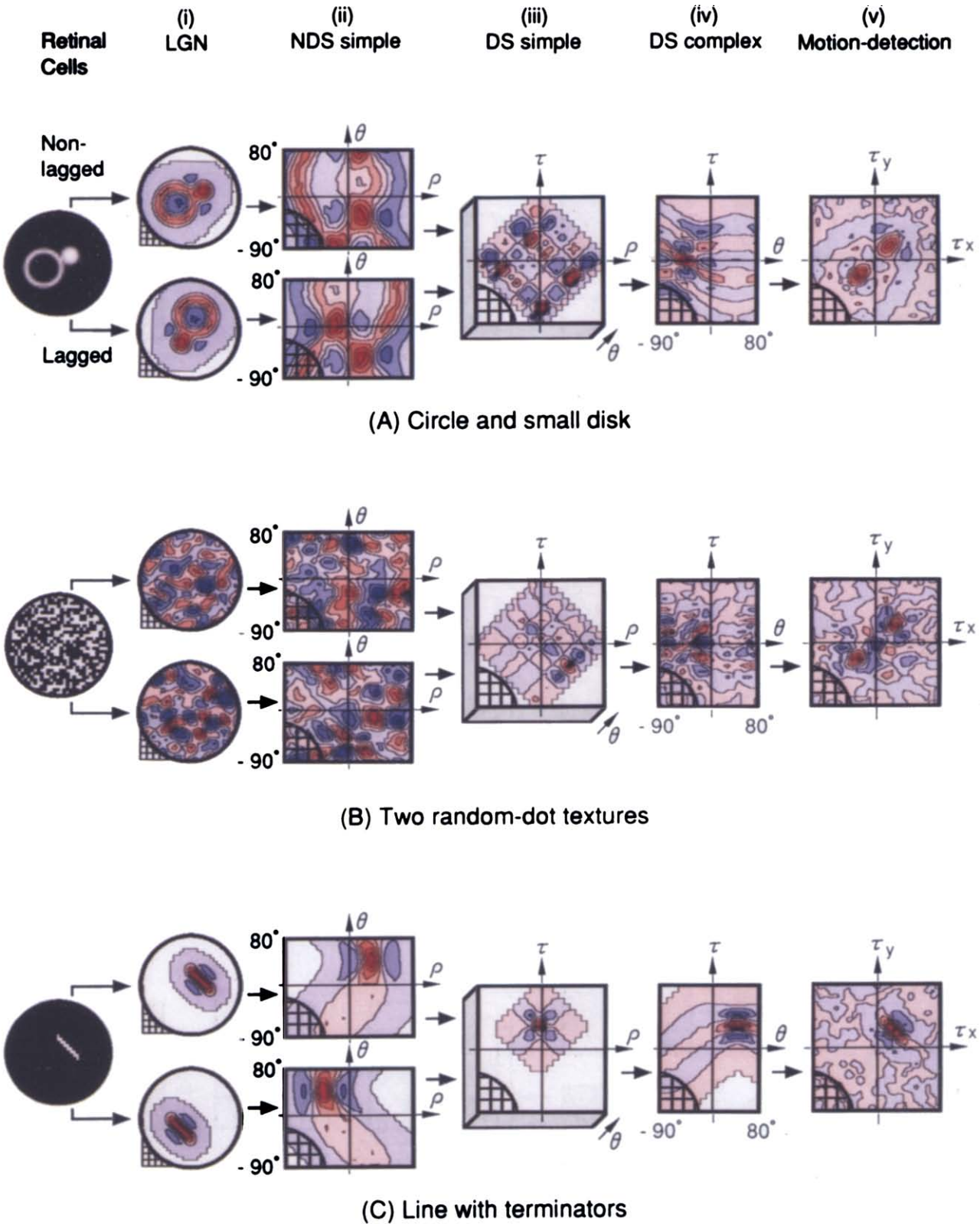

FIGURE 8. (A, B) Sequential processing by the modeled cells to detect 2-D motions from two moving stimuli within a receptive field separately; a circle and a small disk (A) and two random-dot textures (B). (C) The processing to detect 2-D motion from a moving line with terminators. Figures 6–8 are, to our knowledge, the first prediction of such firing patterns in each cell array in response to the stimuli. Optical imaging (Obermayer & Blasdel, 1993; Bonhoeffer & Grinvald, 1993) enables the firing patterns characteristic for each cell and stimulus type to be validated.

whose coordinates coincide with the θ orientations and τ 1-D velocities of the bars fire to detect them. In each case inhibitory subpeaks occur on both sides of the activated cells.

In the motion-detection cell array [Fig. 6A(v)], the cell at ($\tau_x = 3$, $\tau_y = 3$) fires most intensively after extracting a sine wave [equation (10)] that passes through the two activated cells in the (θ, τ) array. The cell corresponds to the intersection of the two lines that are the elementary inverse Hough transformation (Appendix A.2) of the two activated cells. Hence, by inserting this cell's coordinates into equation (13), the 2-D motion of the cross is correctly determined to be $(2/t_d)(3, 3)$. This vector must be multiplied by the interval between adjacent retinal cells (Section 2.3.2).

The modeled cells can detect the 2-D motion of "straight-line figures" that are composed of two or more differently oriented lines. The activation of the motion-detection cell at the intersection [Fig. 6A(v)] is more isolated and sharper when the figure contains more lines.

3.2. Dots

Figure 6B shows how modeled cells detect the 2-D motion of a single dot.

In each NDS simple cell array [Fig. 6B(ii)], a sine wave composed of activated cells occurs accompanied by inhibitory responses on both sides. The wave is the elementary Hough transformation of the dot (Appendix A.1), indicating the ρ locations and θ orientations of all possible lines passing through the dot.

The DS simple and complex cells convert the waves in the lagged and nonlagged NDS simple cell arrays into a sine wave composed of activated DS complex cells over the (θ, τ) array [Fig. 6B(iv); equation (10)]. The wave indicates the θ orientations and τ 1-D velocities of all the lines passing through the dot.

A motion-detection cell at ($\tau_x = 3$, $\tau_y = 3$) is activated to extract this wave, which is surrounded by inhibitory responses [Fig. 6B(v)]. Thus, the 2-D motion of the dot is correctly detected as this cell's coordinates.

The modeled cells can detect the 2-D motion of "dot figures" that are composed of any number of dots. The detection process is the same as that for moving lines composed of all lines passing through the dots within the figures.

The inhibitory responses (blue) in each cell array, which result from the inhibitory concentric receptive fields of LGN cells [the second term of equation (3)], play an important role in suppressing bias and noise. These responses, for example, suppress the group of linear firing patterns [on the left of Fig. A1(ii) in Appendix A] except for a cell at the group's intersection. This results in the isolated activation of the motion-detection cell at the point [e.g. Fig. 6B(v)]. Further, the inhibitory responses suppress the group of sinusoidal firing patterns [on the right of Fig. A1(i)] except for a cell at the group's intersection. This results in the isolated activation of the NDS simple cell at the point [e.g. Fig. 6A(ii)].

3.3. Random-dot Texture

Traditionally, neurophysiological experiments have used random-dot stimuli, which are a kind of dot figure, together with the bar and single-dot stimuli. The modeled cells can detect 2-D motion from a random-dot texture with 30% dot density (Fig. 6C).

NDS simple cells [Fig. 6C(ii)] detect all possible lines passing through every dot within the texture. Because the dots are located randomly, the cell responses look like noise. DS simple cells [Fig. 6C(iii)] fire again and DS complex cells [Fig. 6C(iv)] fuse these random responses. The resultant sine wave composed of activated DS complex cells indicates the θ orientations and τ 1-D velocities of all the lines. To detect the 2-D motion of the texture, the motion-detection cell at ($\tau_x = 3$, $\tau_y = 3$) extracts the wave [Fig. 6C(v)].

Figure 6B and C suggests the neurophysiological process by which type II cells in area MT, which correspond to our motion-detection cells (Section 4.2.2), detect the 2-D motion of moving single and random dots (Albright, 1984^{++}).

3.4. Curved Lines

Figure 7A shows how the 2-D motion of a circle is detected.

In each NDS simple cell array [Fig. 7A(ii)], two sine waves of activated cells occur. The waves indicate the ρ locations and θ orientations of all possible lines tangential to the circle. The interval between the wave in the ρ direction is the circle's diameter (Casasent & Krishnapuram, 1987).

The DS simple and complex cells convert the waves in the lagged and nonlagged NDS simple cell arrays into a sine wave composed of activated DS complex cells over the (θ, τ) array [Fig. 7A(iv)]. The wave flanked by two secondary waves on both sides indicates the θ orientations and τ 1-D velocities of all the lines tangential to the circle. To detect the 2-D motion of the circle, the motion-detection cell at ($\tau_x = 3$, $\tau_y = 3$) extracts the central wave [Fig. 7A(v)].

The modeled cells can detect the 2-D motion of "curved-line figures". The detection process is the same as that for moving lines composed of all lines tangential to the figures.

3.5. Edges

Figure 7B shows how the 2-D motion of a disk is detected.

In each NDS simple cell array [Fig. 7B(ii)], two sinusoidal borders of excitatory/inhibitory cell responses occur. The borders indicate the ρ locations and θ orientations of all possible lines tangential to the disk. The differentiation of the disk edge by the convolution operation [equation (2)] causes this pair of excitatory and inhibitory responses.

The DS simple and complex cells convert the borders in the lagged and nonlagged NDS simple cell arrays into a sine wave composed of activated DS complex cells over the (θ, τ) array [Fig. 7B(iv)]. The wave indicates the θ

orientations and τ 1-D velocities of all the lines tangential to the disk. To detect the 2-D motion of the disk, the motion-detection cell at ($\tau_x = 3$, $\tau_y = 3$) extracts the wave [Fig. 7B(v)].

The modeled cells can detect the 2-D motion of "edge figures". The principal detection process [Fig. 7B(iv, v)] is the same as that for moving lines composed of all lines tangential to the figures.

3.6. Noise Robustness

The modeled cells' 2-D motion detection process is robust to noise.

Figure 7C shows how 2-D motion is detected from a moving circle on which random-dot noise with a 30% dot density is superimposed with temporal incoherence. The noise significantly degrades the NDS simple cell responses [Fig. 7C(ii)] compared to those obtained for circles without noise [Fig. 7A(ii)]. The DS simple and complex cells and motion-detection cells reduce the disturbance, however, and the 2-D motion is correctly detected with little noise degradation [Fig. 7C(v)].

The 2-D motion of stimuli moving with temporal coherence is extracted, whereas that of stimuli moving with temporal incoherence is not extracted. Hence, our 2-D motion detection process is robust to noise.

3.7. Two Stimuli Within a Receptive Field

The modeled cells can detect the 2-D motions from two moving stimuli within a receptive field separately. This is consistent with motion transparency in psychophysiology.

Figure 8A shows how the 2-D motions are detected from a moving circle and moving small disk separately. In the DS complex cell array [Fig. 8A(iv)], two sine waves of activated cells occur over the (θ, τ) array, with one another's amplitudes reversed; a DS complex cell at the intersection of the waves is activated most intensively. One wave indicates the θ orientations and τ 1-D velocities of all lines tangential to the circle; the other indicates those tangential to the disk. Extracting these waves, two motion-detection cells are activated separately [Fig. 8A(v)]. The cell at ($\tau_x = 3$, $\tau_y = 3$) detects the 2-D motion of the disk, and the cell at ($\tau_x = -3$, $\tau_y = -3$) detects that of the circle.

Figure 8B shows how the 2-D motions are detected from two moving random-dot textures. In the motion-detection cell arrays [Fig. 8B(v)], two cells at ($\tau_x = 3$, $\tau_y = 3$) and ($\tau_x = -3$, $\tau_y = -3$) are activated separately to detect the textures' 2-D motions.

3.8. Line with Terminators

The modeled cells can detect the 2-D motion of a line with terminators (Fig. 8C), although they cannot detect that without the terminator because of the aperture problem (Hildreth & Koch, 1987):

In the DS complex cell array [Fig. 8C(iv)], a sine wave of activated cells occurs over the (θ, τ) array, accompanied by an intensively activated cell (detecting the line's 1-D velocity) on it. The wave indicates the θ orientations and τ 1-D velocities of all possible lines passing through the terminators. Accumulating the responses of all the cells along the wave, a motion-detection cell at ($\tau_x = 3$, $\tau_y = 3$) fires most intensively to detect the 2-D motion [Fig. 8C(v)]. Thus, the 2-D motion of this line is detected as that of the terminators. The linear firing pattern passing through the cell corresponds to a constraint line given by the (V_{1D}, θ) 1-D velocity of the line. The pattern length becomes shorter as the line shortens.

Sections 3.1–3.5 indicate that the modeled cells [equations (2, 4, 5, 12, and 14)] can detect the 2-D motion of a variety of stimuli, including dots, straight and curved lines, and edges. The motion detection is independent of the location, orientation, and contrast polarity of these stimuli. This is consistent with neurophysiology (Section 2.1). The 2-D motion detection above is robust to noise (Section 3.6) and capable of measuring the 2-D motions from two moving stimuli separately (Section 3.7).

3.9 Extracting Optical Flow

Figure 9A shows one of two successive frames of a rotating wooden ball. The modeled cells detected the 2-D motion within each receptive field. Figure 9B shows that the optical flow, which was measured for rotation about an axis perpendicular to the paper, is accurately detected, and that the stationary background is detected as flow with length zero. Errors occurs in a few receptive fields for which all the grains have the same orientation, so that the aperture problem can not be solved.

4. COMPARISON WITH NEUROPHYSIOLOGY

The responses of the modeled cells [equations (2, 4, 5, 12, and 14)] for various stimuli are consistent with the following responses of actual cells: first, selectivities to the parameters of traditionally used bar stimuli (Section 4.1); second, the responses of the Component, Pattern, type I, and type II cells to three combinations of stimuli (Section 4.2); third, the receptive-field structures of simple cells (Section 4.3); fourth, the "grain" and "field" cell-responses to the movement of random-dot textures (Section 4.4); and, finally, the cell responses for apparent motion (Section 4.5).

4.1. Selectivities to Bar Stimuli

This section shows that the modeled cells exhibit the same selectivities to the bar stimulus parameters (i.e. ρ location, θ orientation, τ 1-D velocity, and contrast polarity) as actual cells (Table 1).

LGN cells respond selectively to the stimulus' ρ location, based on its contrast polarity, and independent of its θ orientation and τ 1-D velocity (Table 1). The modeled cells having the concentric receptive field [equation (3)] exhibit the same selectivity.

NDS simple cells respond selectively to the bar's ρ location and θ orientation, based on its contrast polarity, and independent of its τ 1-D velocity. The modeled cells arranged as the (ρ, θ) array exhibit the same selectivity (Section 2.2.2); they respond equally in both directions of bar movement. Figure 10A shows a polar plot for an NDS

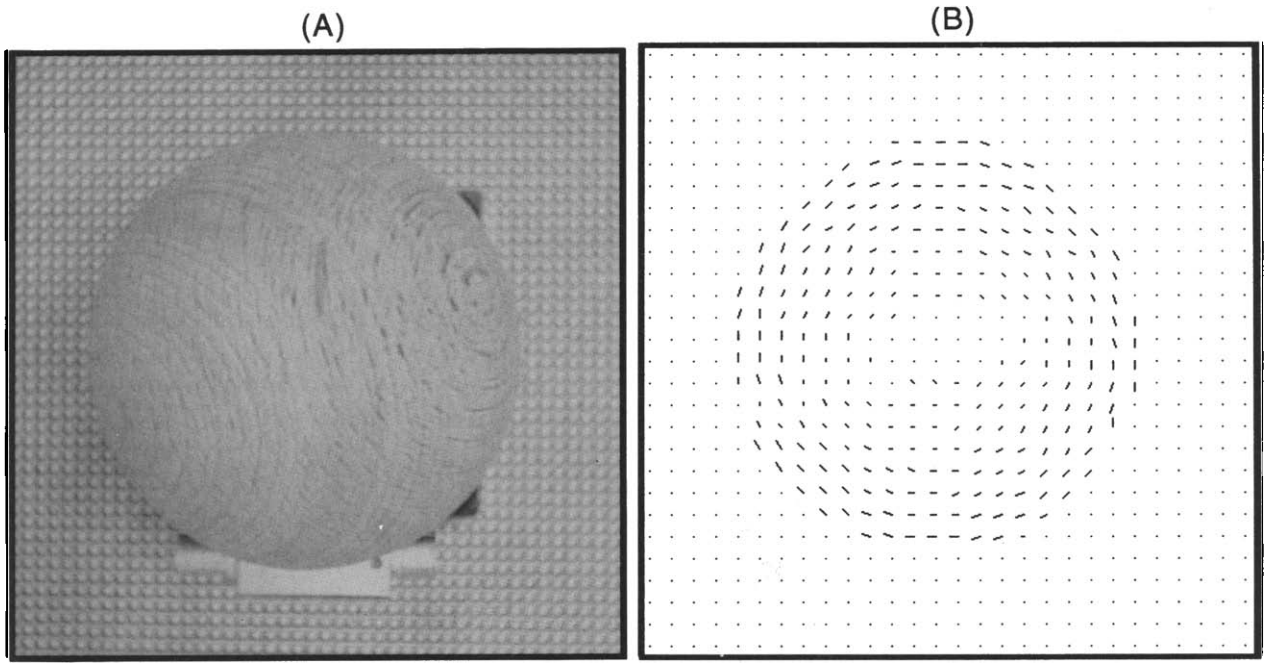

FIGURE 9. (A) One of two successive frames of a rotating wooden ball. The image composed of 512 × 512 retinal cells (or pixels) was divided into circular receptive fields which are 31 cells in diameter, with their centers 16 cells apart. Then, the 2-D motion within each receptive field was detected by the modeled cells [equations (2, 4, 5, 12, and 14)], and depicted as a flow whose length and direction are the motion's speed and direction. (B) Extracted optical-flow field which occurs for the rotation about an axis perpendicular to the paper.

simple cell as an example of orientation selectivity. This plot fits that of an actual simple cell (Fig. 10B).

DS simple cells respond selectively to the bar's ρ location, θ orientation, and τ 1-D velocity, independent of its contrast polarity. The modeled cells arranged as the (ρ, θ, τ) array exhibit the same selectivity (Section 2.2.3). Figure 11A(i) shows a polar plot for a DS simple cell as an example of direction selectivity. This plot showing the unidirectional selectivity fits that of an actual DS simple cell [Fig. 11A(ii)]. Further, to study the velocity selectivity, we plotted the 1-D velocity-tuned curve of the cell for moving bar stimuli [Fig. 11B(i)]. The main peak, whose τ coordinate gives the cell's preferred 1-D velocity as $2\tau/t_d$, resembles that of the actual DS simple cell [Fig. 11B(ii)]. The two subpeaks result from the inhibitory concentric receptive field of LGN cells [i.e. the second term of equation (3)]. Replacing the τ velocity in equation (5) with $\log_a \tau$ allows us to use a log scale for the abscissa.

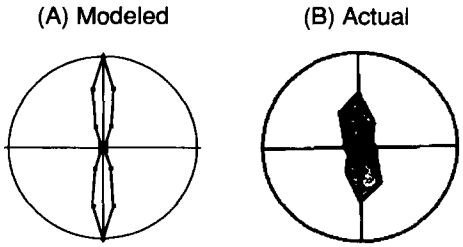

FIGURE 10. (A) The polar plot of orientation selectivity of a modeled NDS simple cell at ($\rho = 0$, $\theta = 90$ deg) for stationary bar stimuli. Using equation (4), we calculated the orientation selectivity of the cell. Then, we depicted the selectivity as a polar plot whose radius and angle are the cell response and bar orientation. (B) The plot of an actual simple cell taken from Wörgötter and Eysel (1989⁺).

DS complex cells respond selectively to the bar's θ orientation and τ 1-D velocity, independent of its ρ location and contrast polarity. The modeled cells arranged as the (θ, τ) array exhibit the same selectivity (Section 2.3.1). The modeled cell's direction and velocity selectivities for bar stimuli, not shown here, are almost the same as those of the DS simple cells [Fig. 11A(i) and B(i)], and are consistent with those of actual DS complex cells in cats (Hammond & Reck, 1980; Hammond & Smith, 1983; Baker, 1988).

Finally, motion-detection cells respond selectively to the bar's θ orientation and τ 1-D velocity, independent of its ρ location and contrast polarity. The modeled cells exhibit the same selectivity. Since the selectivities of motion-detection cells for bar stimuli are the same as those of DS complex cells (Table 1), it is difficult to distinguish between these cell types using only bar stimuli. The next section shows three methods for distinguishing between them using more complex stimuli.

4.2. Direction and Orientation Selectivities

This section shows that the modeled DS complex cells reflect the direction and orientation selectivities in the Component and type I cells for the three combinations of stimuli below; it also shows that the modeled motion-detection cells reflect the selectivities in the Pattern and type II cells. The first stimulus is a combination of the moving grating and plaid, and is used to distinguish between Component and Pattern cells (Movshon *et al.*, 1985; Rodman & Albright, 1989) (Section 4.2.1). The second stimulus is a combination of the stationary bar and the moving bar and dot, and is used to distinguish between type I and type II cells (Albright,

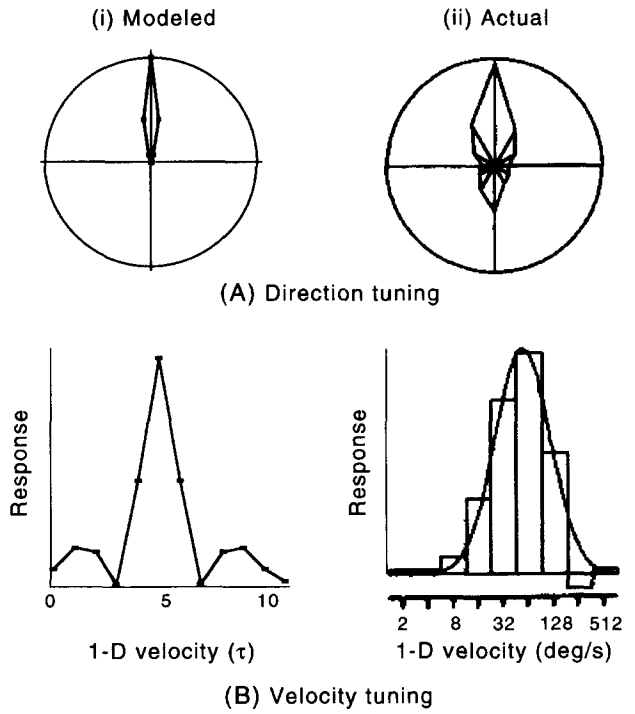

FIGURE 11. (A) Polar plots of direction selectivities of modeled and actual DS simple cells for moving bar stimuli. (i) Using equation (5), we calculated the selectivity of a modeled cell at ($\rho = 0$, $\theta = 90$ deg, $\tau = 5$) for bar stimuli moving with a speed of $\tau = 5$. Then, we depicted the result as a polar plot whose radius and angle are the cell response and direction of bar movement. (ii) The actual plot is taken from Wörgötter and Eysel (1989+). (B) Velocity tuning curves for the modeled and actual cells. The actual curve is taken from Baker (1988+).

1984; Rodman & Albright, 1989) (Section 4.2.2). The third stimulus is a combination of moving bar and dot stimuli with differing speeds, and is used to identify DS complex cells in area V1 (e.g. Hammond & Reck, 1980) and type II cells in area MT (Albright, 1984) (Section 4.2.3).

4.2.1. Gratings and plaid patterns

To distinguish between Component and Pattern cells in area MT of monkeys, Movshon *et al.* (1985) measured the difference in the direction tunings for a combination of a moving sinusoidal grating and plaid. The Component cell's direction tuning was bimodal for the plaid; the optimal directions occurred when the component gratings were roughly perpendicular to the cells' preferred direction for single gratings. In contrast, the optimal direction of the Pattern cells for the plaid was approximately coincident with that for the single gratings.

Figure 12 shows the direction tunings of the modeled DS complex and motion-detection cells for the grating and plaid stimuli. The optimal directions for these tunings fit the experimental observations. This suggests that our DS complex and motion-detection cells correspond to the Component and Pattern cells.

4.2.2. Stationary and moving stimuli

To distinguish between type I and type II cells in area MT of monkeys, Albright (1984) measured the difference in the orientation and direction tunings for a combination of a stationary bar and a moving bar and dot. Type I cells exhibit the perpendicular relationship between their preferred orientation tunings (for stationary bars) and direction tunings (for moving bars and dots), whereas type II cells exhibit the parallel relationship. Rodman and Albright (1989+) and Albright, Rodman and Gross (1986+) clarified that these type I and type II cells correspond to the Component and Pattern cells.

Figure 13 shows the orientation and direction tunings of the modeled DS complex and motion-detection cells for this stimulus combination. The perpendicular relationship of the DS complex cell tuning between the preferred orientation and direction is the same as that of type I cells reviewed above. The parallel relationship of the motion-detection cell tuning is the same as that of type II cells. This suggests that our DS complex and motion-detection cells correspond to the type I and type II cells.

4.2.3. Bar and dot with differing speeds

Our modeled cells account for the two types of bimodal direction tuning occurring for a combination of moving bar and dot stimuli with differing speeds. The first type is characteristic of DS complex cells in area V1 of cats (Hammond, 1978; Hammond & Reck, 1980; Hammond & Smith, 1983; Skottun, Grosof & De Valois, 1988) and the second type is characteristic of type II cells in area MT of monkeys (Albright, 1984).

4.2.3.1. DS complex cells in area V1. The direction tuning of DS complex cells in area V1 is unimodal when stimulated with bars or low-speed random-dot textures, but bimodal for high-speed random-dot textures. The two

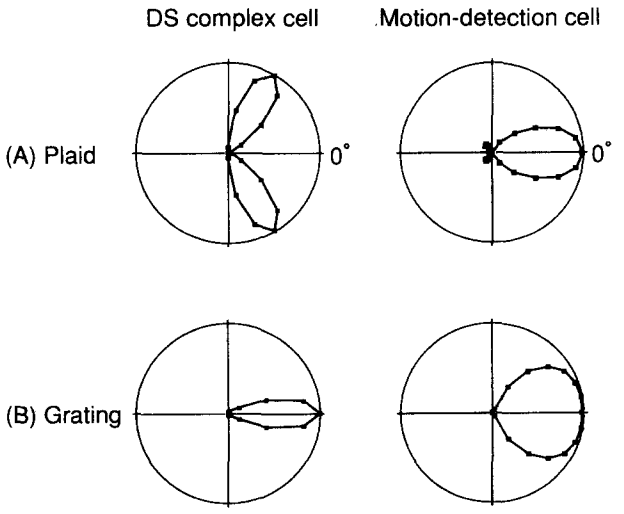

FIGURE 12. Polar plots of direction selectivities of modeled DS complex and motion-detection cells for moving gratings and plaid patterns. The plaid pattern is composed of two differently oriented sinusoidal gratings traveling at an angle of 120 deg to one another and with the same velocity. Using equation (12) and equation (14), we calculated the direction selectivities. Then, we depicted the selectivities as individual polar plots whose radius and angle are the normalized cell response and the stimulus-movement direction. The DS complex cell's direction tuning is bimodal for the plaids; the optimal directions occur when the component gratings are perpendicular to the cell's preferred direction for single gratings. In contrast, the optimal direction of the motion-detection cell for the plaid coincides with that for single gratings.

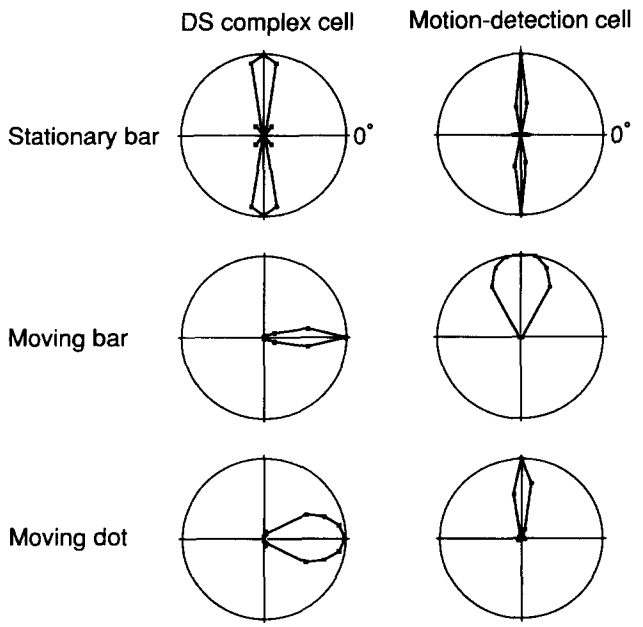

FIGURE 13. Polar plots of orientation selectivities (for stationary bar stimuli) and direction selectivities (for moving bar and single-dot stimuli) of modeled DS complex and motion-detection cells. Using equations (12) and (14), we calculated the selectivities for these stimuli. Then, we depicted the selectivities as an individual polar plot whose radius is the normalized cell response. The plot's polar angles for a stationary bar and for a moving bar or dot are, respectively, bar orientation and the direction of movement for the bar or dot. The DS complex cell exhibits a perpendicular relationship between its preferred orientation and direction, whereas the motion-detection cell exhibits a parallel relationship. [For easy comparison of the orientation selectivity with that observed by Albright (1984$^{+\,+}$) and Rodman and Albright (1989$^{-\,-}$), the bar orientation is plotted with an addition of 90 deg to its definition (Fig. 2A). Also note that the intensities of the DS complex cell responses for the stationary bars are weak, with the exception of cells whose τ coordinates are 0, because the cells prefer the moving bar stimuli. This is consistent with electrophysiology (Maunsell & Van Essen, 1983a$^{+\,-}$; Albright, 1984$^{+\,+}$.]

preferred directions are distributed symmetrically about the bar's preferred direction. The interval between these directions grows wider as the texture speed increases.

Figure 14A shows the direction tuning curves of our DS complex cell for bar and dot stimuli moving with different speeds. We used single-dot stimuli which cause the same direction tunings as the random-dot stimuli used in the experiments. The unimodal and bimodal tunings fit the experimental observations. The $\Delta\theta_{CC}$ interval between the twin peaks of bimodal tuning is a function of the dot speed V_{dot} and the preferred speed for a bar V_{1D0}:

$$\Delta\theta_{CC} = 2\cos^{-1}(V_{1D0}/V_{dot}). \tag{15}$$

In addition, our DS simple cells [equation (5)] exhibited almost the same unimodal and bimodal tunings, not shown here, as the DS complex cells (Fig. 14A). The interval between the twin peaks varied as predicted by equation (15). This is consistent with observations of DS simple cells (Skottun *et al.*, 1988^{+}).

4.2.3.2. Type II cells in area MT. The direction tuning of type II cells in area MT is unimodal when stimulated with single dots or high-speed bars, but bimodal for low-speed bars (Albright, 1984$^{+\,+}$). The two preferred directions are distributed symmetrically about the dot's preferred direction. The interval between these directions grows wider as the bar speed decreases. Rodman and Albright (1987$^{+\,+}$), however, failed to replicate these results. Of the 13 type II cells they examined, only one exhibited the bimodal direction tuning. In contrast, of the type II cells examined by Albright (1984), 39% exhibited the bimodal direction tuning.

Figure 14B shows the direction tuning curves of our motion-detection cells, which correspond to the type II cells (Section 4.2.2), for bar and dot stimuli moving with the different speeds. The unimodal and bimodal tunings fit the experimental observations (Albright, 1984). The $\Delta\phi_{MDC}$ interval between the twin peaks of bimodal tuning is a function of the bar speed V_{bar} and the preferred speed for a dot V_{2D0}:

$$\Delta\phi_{MDC} = 2\cos^{-1}(V_{bar}/V_{2D0}). \tag{16}$$

This suggests that our DS complex and motion-detection cells account for the neurophysiological tuning process and the dependence of the bimodal tuning type on the speeds of the moving bar and dot. We note that a formula equivalent to equation (16) was derived by Albright (1984) based on the IOC solution, whereas equation (15) has, to our knowledge, not yet been reported.

Finally, we predict that the Component and type I cells in area MT, which correspond to our DS complex cells (Section 4.2.1 and Section 4.2.2), have the same bimodal tunings as the DS complex cells in area V1 (Fig. 14A).

4.3. Receptive-field Structure

Two receptive-field structures of simple cells in area V1 of cats were examined (Hubel & Wiesel, 1959, 1962; Movshon, Thompson & Tolhurst, 1978a; Jones & Palmer, 1987a,b). The first structure is possessed by simple cells preferring line stimuli, which we call line-preferring simple cells. The second structure is possessed by simple cells preferring edge stimuli, which we call edge-preferring simple cells. Our NDS simple cells [equation (4)] and a modification of them account for the two structures.

4.3.1. Line-preferring simple cell

The receptive-field structure of an actual line-preferring simple cell [Fig. 15A(i)] consists of an elongated, excitatory region flanked by two inhibitory regions.

The simulated receptive-field structure of a modeled NDS simple cell [Fig. 15A(ii)] is consistent with the actual structure. The cell's (ρ, θ) coordinates give the ρ location and θ orientation of the elongated excitatory region. This structure results from the Hough transformation of the DOG(x, y) function [equations (2–4)], which is executed within the rectangular receptive field [Fig. A2(ii) in Appendix A].

4.3.2. Edge-preferring simple cell

The receptive-field structure of an actual edge-preferring simple cell [Fig. 15B(i)] consists of a pair of elongated, excitatory and inhibitory regions.

We show that this observation is consistent with the receptive-field structure of a modified NDS simple cell, as follows.

We model the responses of an edge-preferring simple cell in equation (17) as the difference between the NDS simple cell responses [equation (4)] along the ρ coordinate, introducing a parameter χ:

$$SC_{NDS,\,EDGE}(\rho, \theta) = SC_{NDS}(\rho + \chi, \theta) - SC_{NDS}(\rho - \chi, \theta). \quad (17)$$

We assume that the edge-preferring simple cells are arranged in layer 4B of area V1 as the (ρ, θ) array. This arrangement is the same as that of modeled NDS simple cells (Section 6.1). Equation (17) indicates that an edge-preferring simple cell at (ρ, θ) fires to detect an edge $\rho = x\cos\theta + y\sin\theta$ in the (x, y) LGN cell array.

The simulated receptive-field structure of this edge-preferring simple cell [Fig. 15B(ii)] is consistent with the actual structure. The cell's (ρ, θ) coordinates give the ρ location and θ orientation of the border of the structure, i.e. those of the border of the elongated, excitatory and inhibitory regions. This structure results from the Hough transformation, above, followed by the first differential along the ρ coordinate [equation (17)].

We note that replacing the NDS simple cells [equation (4)] in our cell sequence [equations (2, 4, 5, 12, and 14)] with edge-preferring simple cells [equation (17)] does not significantly change the responses in the DS complex and motion-detection cells. Hence, this replaced cell sequence can detect the 2-D motion of moving stimuli in the same way as the original sequence.

4.3.3. Similarity to 2-D Gabor functions

Daugman (1985) proposed that the receptive-field structures of line- and edge-preferring simple cells resemble 2-D even and odd Gabor functions. This similarity was validated by detailed experiments (Jones & Palmer, 1987b+).

These structures are characterized by their cross-sections. As Fig. 16 shows, the cross-sections of the structures possessed by modeled line-and edge-preferring simple cells resemble those of the 2-D even and odd Gabor functions. Hence, these modeled cells possess the structure resembling the two types of 2-D Gabor function.

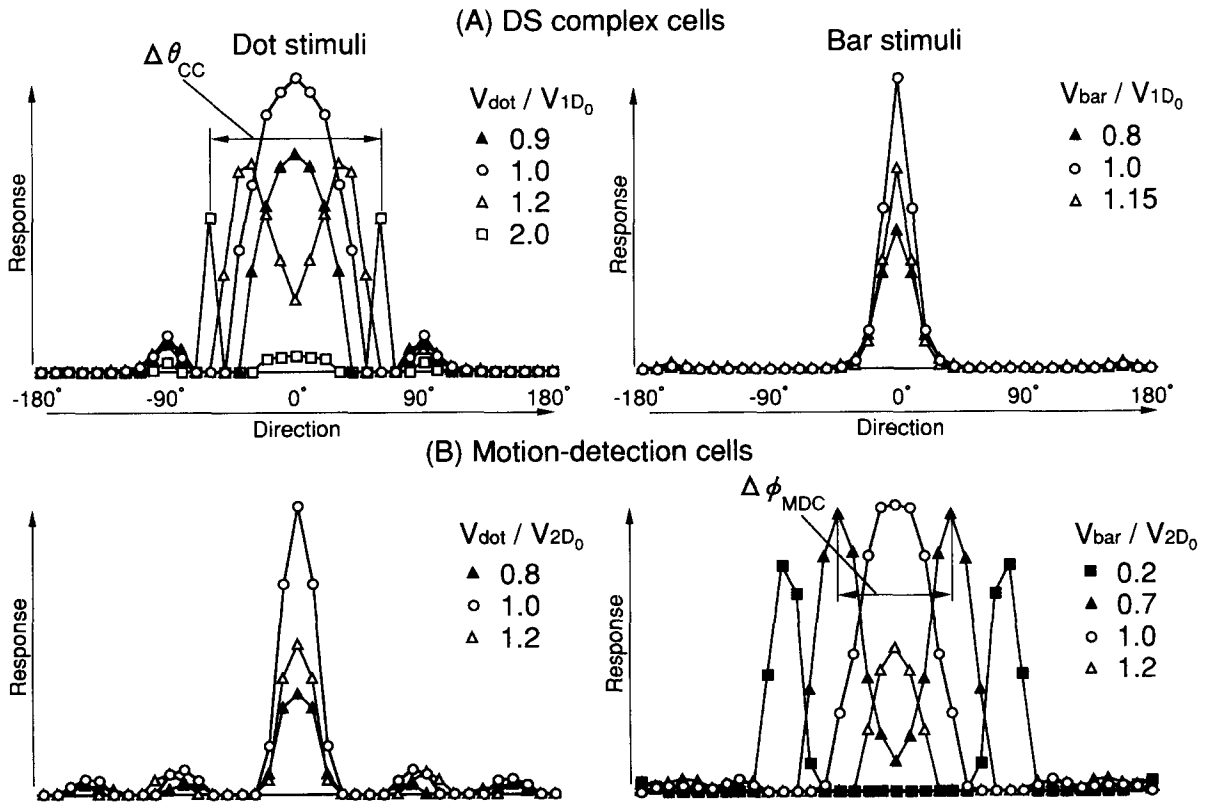

FIGURE 14. Direction tuning curves of modeled DS complex and motion-detection cells for bars and single dots with the differing V_{bar} and V_{dot} speeds. Using equations (12) and (14), we calculated the direction selectivities for these stimuli. Then, we depicted the selectivities with the abscissa showing the direction of stimulus movement and the ordinate showing the cell response. (A) Unimodal direction tunings occur for bars and low speed dots, with an optimal bar speed V_{1D0} that is given as $2\tau/t_d$ based on the cell's (θ, τ) coordinates. In contrast, bimodal tunings occur for dots with speeds higher than the V_{1D0} optimal speed. The twin peaks of bimodal tuning are distributed symmetrically about the bar's preferred direction. The interval between the peaks $\Delta\theta_{CC}$ widens as the dot speed increases [equation (15)]. (B) Unimodal direction tunings occur for dots and high-speed bars, with an optimal dot speed V_{2D0} that is given as $(2/t_d)\sqrt{(\tau_x^2 - \tau_y^2)}$ based on the cell's (τ_x, τ_y) coordinates. Bimodal tunings occur for bars with speeds lower than the V_{2D0} optimal speed. The twin peaks of bimodal tuning are distributed symmetrically about the dot's preferred direction. The interval between the peaks $\Delta\phi_{MDC}$ widens as the bar speed decreases [equation (16)].

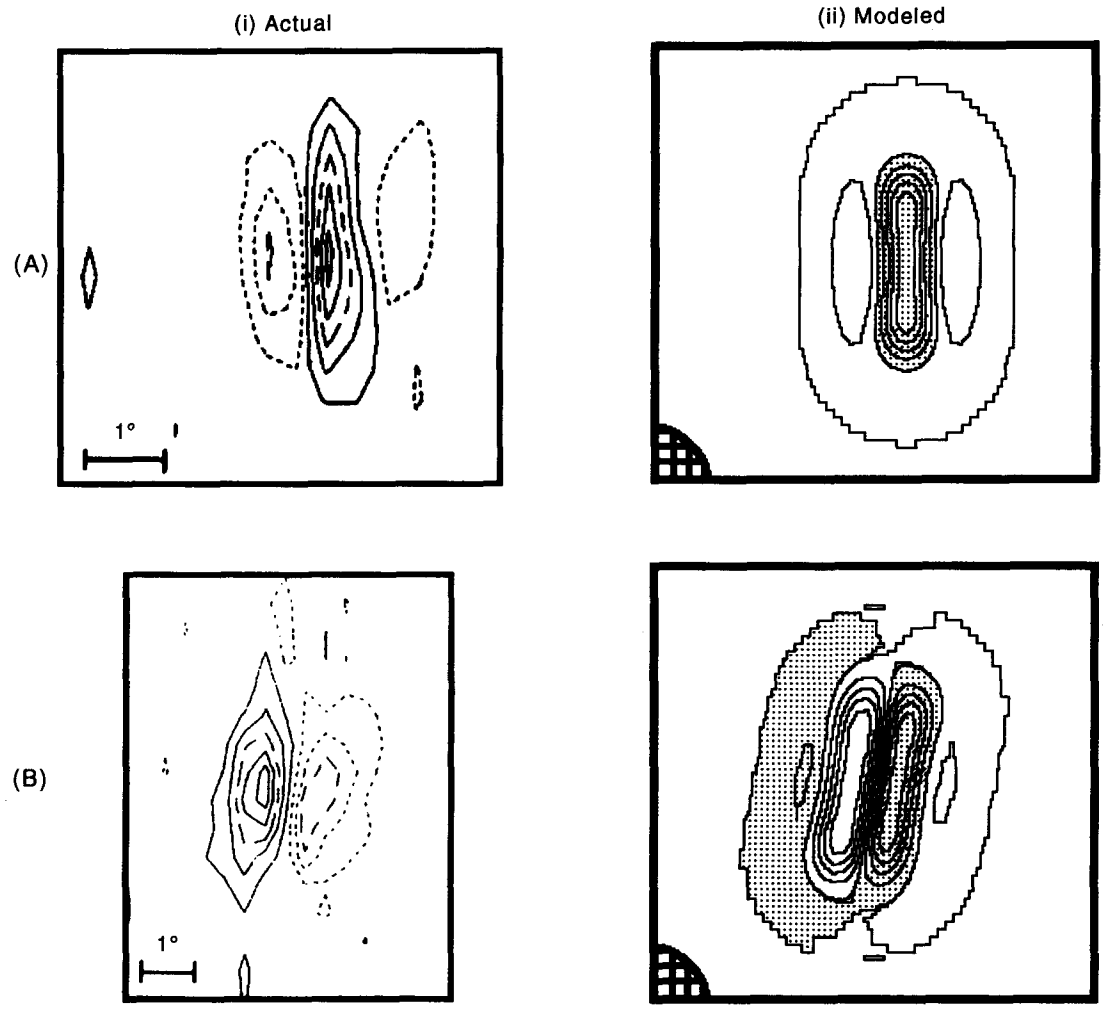

FIGURE 15. Receptive field structures of (A) line-and (B) edge-preferring simple cells. (i) The structures of actual cells in area V1 quoted from Jones and Palmer (1987b+), which were measured using the reverse correlation technique developed by Jones and Palmer (1987a+). Cell responses for the differing locations and contrast polarity of dot stimuli were depicted as a contour map whose address corresponds to a dot location. Solid and dotted lines represent excitatory and inhibitory responses corresponding to dot's contrast polarity. (ii) The structures of a modeled line-preferring simple cell (i.e. a modeled NDS simple cell) at ($\rho = 4$, $\theta = 0$) and an edge-preferring simple cell at ($\rho = 0$, $\theta = -10$ deg). Using equation (4) and equation (17), cell responses for the differing locations and contrast polarity of dot stimuli are calculated, then depicted as contour maps. Hatched and nonhatched regions represent excitatory and inhibitory responses, and each lattice point in the lower left corner of the map corresponds to 2 × 2 retinal cells. The χ parameter in equation (17) has a value 2, and the other parameters used for the simulation are shown in Appendix B.

4.4. "Grain" and "Field" Responses

The grain and field responses to the movement of random-dot textures have been examined previously (Hammond & MacKay, 1977+; Gulyas, Orban, Duysens & Maes, 1987+; Snowden, Treue & Andersen, 1992++). The grain response does not last for the whole duration of the texture motion. It produces one or more peaks similar to those elicited by a moving bar. In contrast, the field response lasts for the same time as the texture motion. The researchers observed the grain responses for all LGN cells and nearly all V1 cells, and the field responses for smaller V1 cells and nearly all MT cells. Simple and complex cells tend to exhibit the grain and field responses. We note that the complex cell type includes our motion-detection cell.

The simulated responses of the modeled cells to the movement of a random-dot texture are consistent with these experimental observations. As shown in Fig. 17, the DS complex and motion-detection cells exhibited the field responses, and the DS simple cell exhibited the grain responses. The LGN and NDS simple cells, not shown here, exhibited the grain responses.

Our cell model accounts for these responses as follows.

The movement of a random-dot texture causes a grain response in NDS and DS simple cells, because the cells are sensitive to the locations and orientations of lines that pass through the dots within the texture. The grain responses also occur in LGN cells because the cells are sensitive to the dots' locations.

In contrast, field responses occur in motion-detection cells because the cells' responses are independent of the texture's location (Section 3.8). DS complex cells, which are insensitive to the lines' locations, exhibit the field

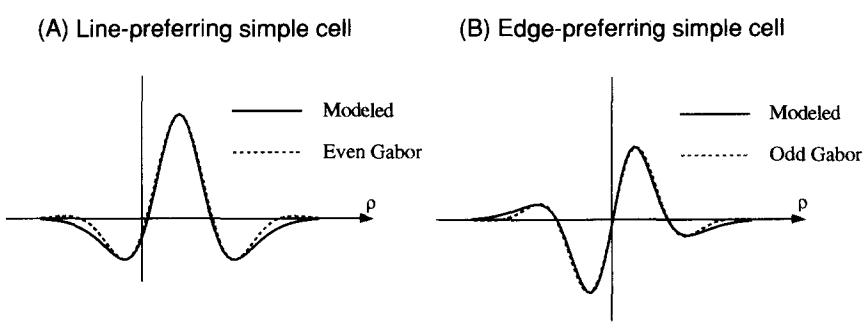

FIGURE 16. Cross-sections of the receptive field structures [Fig. 15(ii)] possessed by the modeled simple cells and those of the 2-D Gabor functions. The structures and functions are cut perpendicularly to them through their centers. (A) The solid curve shows the cross-section of the structures [Fig. 15A(ii)] possessed by the modeled line-preferring simple cell at ($\rho = 4$, $\theta = 0$). This curve equals the orthogonal projection of the DOG(x, y) function on a line. The dotted curve shows the cross-section of a 2-D even Gabor function shifted by 4 in the ρ direction, $\cos(c_1(\rho - 4))\ \exp\{-[c_2(\rho - 4)]^2\}$; c_1 and c_2 are constants. (B) The solid curve shows the cross-section of the structures [Fig. 15B(ii)] possessed by the modeled edge-preferring simple cell at ($\rho = 0$, $\theta = -10$ deg). This curve equals the orthogonal projection, above, differentiated by equation (17). The dotted curve shows the cross-section of a 2-D odd Gabor function, $\sin(c_3\rho)\ \exp[-(c_4\rho)^2]$; c_3 and c_4 are constants. (Note that the axis of the cross-section corresponds to the ρ axis of these simple cell arrays.)

responses. The response fluctuates (Fig. 17B) because the cells are sensitive to the lines' orientations.

4.5. Apparent Motion

Actual DS cells respond selectively to apparently moving bar stimuli, i.e. bar stimuli flashed successively at temporally and spatially separated intervals, such as movies. This response is the same as that for continuously moving bar stimuli. Researchers examined such apparent-motion responses of DS cells in areas V1 of cats (Movshon, Thompson & Tolhurst, 1978b; Baker, 1988; Baker & Cynader, 1986, 1988) and MT of monkeys (Mikami, Newsome & Wurtz, 1986a,b; Newsome, Mikami & Wurtz, 1986). Further, Mikami (1991) showed that 82% of the DS cells in area MT of monkeys exhibit directional responses to apparent motion of both random-dots and bars.

Our modeled DS simple and complex cells and motion-detection cells also respond selectively to apparent motion in the same way as continuous motion. The simulated motion-detection process for continuously moving stimuli (Figs 6–8) is the same as that for apparently moving stimuli, because the lagged and nonlagged LGN cell images for continuous motion [e.g. Fig. 6A(i)] coincide with the two images flashed successively for apparent motion.

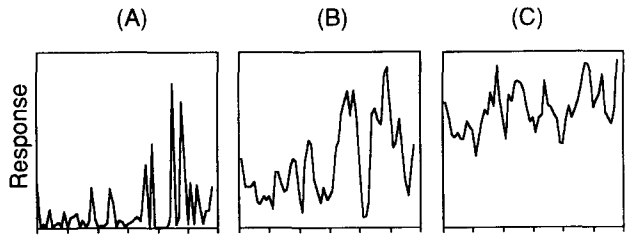

FIGURE 17. "Grain" and "field" responses of (A) a modeled DS simple cell, (B) a DS complex cell, and (C) a motion-detection cell, for the movement of the same random-dot texture as for Fig. 6C. The abscissa is the texture's location and the ordinate is the cell response. The DS simple and motion-detection cells exhibit the grain and field responses. The DS complex cell exhibits the field responses with some fluctuations.

To study apparent-motion detection, Baker and Cynader (1988$^+$) used two successive flashing bar stimuli with differing $\Delta\rho$ spatial and Δt temporal intervals. Unlike in other experiments (Emerson, Citron, Vaughn & Klein, 1987$^+$; Emerson, Bergen & Adelson, 1992$^+$), they located the stimuli symmetrically on either side of the cell to be examined. They depicted the responses of simple and complex cells in area V1 as a contour map whose coordinates are the $\Delta\rho$ and Δt intervals. The map had a peak whose $\Delta\rho_0$ and Δt_0 coordinates were 0.3–0.6 deg and 60–90 msec.

The contour map of a modeled DS simple cell for the same stimuli as in Baker and Cynader's (1988) experiments also had a peak. The peak's $\Delta\rho_0$ and Δt_0 coordinates coincide with double the cell's τ coordinate and the t_d time delay of lagged LGN cells. The V_{1D} velocity of a continuously moving bar, preferred by this cell, is given as $\Delta\rho_0/\Delta t_0$ ($=2\tau/t_d$). This is consistent with the experimental relationship $V_{1D} = D_{opt}/I_T$ [Fig. 14 of Baker (1988$^+$)]; D_{opt} is our $\Delta\rho_0$ and I_T corresponds to t_d.

Based on this discussion, we predict that the optimal response to apparent motion occurs when the Δt temporal interval coincides with the t_d time delay. An experimental correspondence between the Δt_0 optimal interval observed (60–90 msec) and the t_d time delay of lagged LGN cells (40–80 msec) measured by Mastronarde (1987a$^+$) supports our prediction.

The distribution of time delays, indicating that a lagged LGN cell has a constant time delay within the range, causes the distribution of 1-D velocities preferred by DS simple cells, because the velocity is inversely proportional to the delay. This distorts the sinusoidal firing pattern over the DS complex cell array [equation (10)]; the pattern is the conversion of the 2-D motion of a stimulus by the sequential processing [equations (2, 4, 5, and 12)]. Hence, we assume that, to prevent the distortion and detect the 2-D motion correctly, lagged LGN cells within a circular receptive field [Fig. A2(i) in Appendix A] have the same time delay.

The map of the modeled DS complex cells is almost the

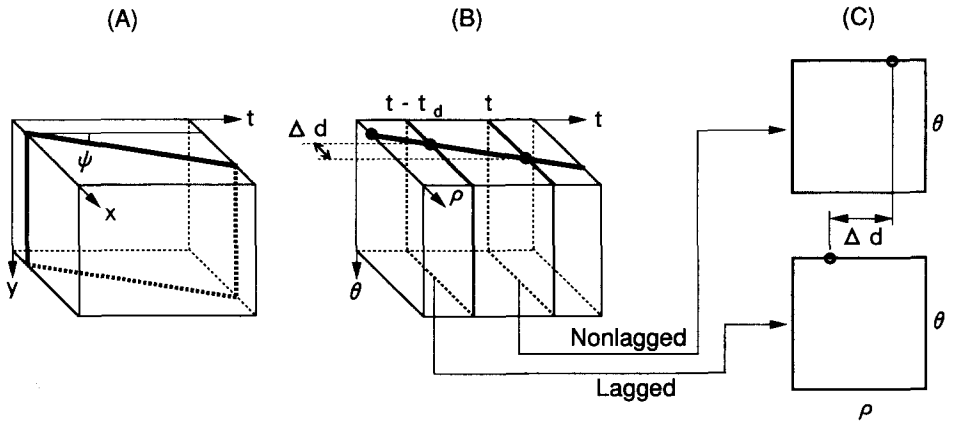

FIGURE 18. Comparison with 1-D velocity detection using the spatio-temporal scheme (Adelson & Bergen, 1985). (A) The scheme uses a (x, y, t) space–time cube. The movement of a line in the (x, y) image plane becomes a slanted planar-locus in the (x, y, t) cube. The planar locus is extracted using spatio-temporal oriented filters, such as the space–time Gabor function (Adelson & Bergen, 1985; Heeger, 1987; Grzywacz & Yuille, 1990). The slope ψ of the locus gives the line's V_{1D} 1-D velocity as $\tan \psi$. (B) To compare this detection process with ours, we modify the (x, y, t) cube to form a space–time cube (ρ, θ, t) by converting the (x, y) image plane into the (ρ, θ) Hough plane. A line in the (x, y) plane is transformed to a spot in the (ρ, θ) plane whose coordinates coincide with the line's ρ location and θ orientation. For example, a vertical line in the image plane is transformed to a bold dot on the ρ axis. Thus, the planar locus in the (x, y, t) cube is transformed to a linear locus on a (ρ, t) slice at a θ coordinate corresponding to the line's orientation. The ψ angle between the linear locus and the t axis gives the line's V_{1D} velocity as $\tan \psi$. (C) The (ρ, θ) slices of this cube at $t - t_d$ and t coordinates are our (ρ, θ) arrays of lagged and nonlagged NDS simple cells; t_d is the fixed time delay of lagged LGN cells. The Δd difference between the arrays' ρ coordinates is proportional to the slope of the linear locus. Performing the spatio-temporal correlation between these simple cell arrays (i.e. between the (ρ, θ) slices), our DS complex cell [equation (12)] determines the 1-D velocity of the line as $\Delta d/t_d$.

same as that of the DS simple cells. The map of the modeled motion-detection cells also has a peak whose Δt_0 coordinate is the t_d time delay. The peak's $\Delta\rho_0$ coordinate, however, depends on the bar stimulus' orientation θ_{bar} and is expressed as $2(\tau_{x0}\cos\theta_{bar} + \tau_{y0}\sin\theta_{bar})$ based on the cell's (τ_{x0}, τ_{y0}) coordinates. This detailed property has not been examined electrophysiologically, to our knowledge.

5. COMPARISON WITH PREVIOUS MODELS

5.1. Two-stage Hypothesis

We compare the two-stage hypothesis (Adelson & Movshon, 1982) to our five types of cell [equations (2, 4, 5, 12, and 14)].

In the first stage of the hypothesis, the (V_{1D}, θ) 1-D velocities of oriented components within a moving stimulus are measured independent of their location and contrast polarity (Adelson & Movshon, 1982; Sereno, 1993). The sequential processing by our LGN cells, NDS and DS simple cells, and DS complex cells measures the 1-D velocities with the same independence.

In the second stage, 2-D motion of the stimuli are measured by combining the velocities using the IOC solution. This solution is equivalent to the inverse Hough transform processed in our motion-detection cells (Section 2.3.2).

Hence, our five cell types provide a neurophysiological explanation to the two-stage hypothesis proposed psychophysically.

Our model accounts for two terms essential to this hypothesis (Fig. 4): The "velocity space (V_x, V_y)" is the same as our (τ_x, τ_y) motion-detection cell array, excluding the coefficient $t_d/2$ [equation (11)]. In addition, the "constraint line", having V_{1D} foot and θ angle, corresponds to a line composed of activated motion-detection cells over the motion-detection cell array (e.g. Fig. 5D). This linear firing pattern is the elementary inverse Hough transformation of a DS complex cell at $(\theta, t_d V_{1D}/2)$.

5.2. Spatio-temporal Method

Heeger (1987) and Grzywacz and Yuille (1990) presented methods for detecting 2-D motion, based on the spatio-temporal scheme (Adelson & Bergen, 1985). The two stages in this method correspond to those in Adelson and Movshon's (1982) hypothesis. The first stage uses spatio-temporal energy filters (Adelson & Bergen, 1985) to measure motion energies that correspond to the 1-D velocities of the oriented components. The second stage combines these energies to detect 2-D motion. This section shows that these two stages correspond to our five cell types.

5.2.1. The first stage

The first stage of Heeger (1987) and Grzywacz and Yuille (1990) uses the (x, y, t) space–time cube (Adelson & Bergen, 1985) to detect the 1-D velocities of lines. Figure 18 shows that the detection process in this cube is equivalent to the spatio-temporal correlation processed in our DS simple cells. Thus, the 1-D velocity detection in the first stage corresponds to the sequential processing by our LGN cells, NDS and DS simple cells, and DS complex cells [equations (2, 4, 5, and 12)]. We added the DS complex cells to the processing, because the detection process in this stage is independent of the lines' locations.

Heeger (1987) and Grzywacz and Yuille (1990)

executed this detection, not in the (x, y, t) cube, but in its frequency domain $(\omega_x, \omega_y, \omega_t)$. Using spatio-temporal energy filters, they measured the motion energies $N(\omega_x, \omega_y, \omega_t)$ that are a representation of the 1-D velocities in the frequency domain. Therefore, their first stage corresponds to our sequential processing in the frequency domain.

5.2.2. *The second stage*

In the first stage, a stimulus moving with (V_x, V_y) 2-D motion produces a group of $N(\omega_x, \omega_y, \omega_t)$ motion energies on a plane [equation (18)] that passes through the origin of the frequency domain (Watson & Ahumada, 1985; Heeger, 1987; Grzywacz & Yuille, 1990):

$$\omega_x V_x + \omega_y V_y + \omega_t = 0. \quad (18)$$

To detect the (V_x, V_y) 2-D motion, their second stage extracts this plane by combining the motion energies lying on it.

Equation (18) is a representation of equation (7) in the frequency domain. Equation (7) is equivalent to equation (10) (Section 2.3.1). Thus, equation (18) is a representation of equation (10) in the frequency domain. This relationship indicates that extracting the plane [equation (18)] in the $(\omega_x, \omega_y, \omega_t)$ coordinate system is equivalent to extracting a sine wave [equation (10)] composed of activated DS complex cells over the (θ, τ) array. Hence, the second stage of Heeger (1987) and Grzywacz and Yuille (1990) corresponds to our motion-detection cells which extract the sine wave using the inverse Hough transform.

5.2.3. *Physiological plausibility*

These methods proposed by Heeger (1987) and Grzywacz and Yuille (1990) give accurate 2-D motion estimates for moving plaid patterns and textured patterns. The methods account for the electrophysiological data on the V1 and MT cells; the space–time separability, direction tuning, apparent motion, and Component and Pattern responses. They also account for the psychophysical data on coherence of plaids.

Grzywacz and Yuille (1990) pointed out, however, that both their method and Heeger's method make two assumptions that are probably incorrect in physiological details. They used Gabor-function models for simple cell receptive fields (Daugman, 1985; Jones & Palmer, 1987b) as spatio-temporal oriented filters for detecting the planar locus (Fig. 18A). In addition, to measure the motion energies independent of the stimulus' contrast polarity, they used the square of the filter outputs as cell responses.

We described all our modeled cells using the synaptic functions of neurons (Section 2.4). We did not use both the Gabor-function-type oriented filters and the square of the filter outputs.

In the sections that follow, we compare our cell sequence to three other methods for detecting 2-D motion using the inverse Hough transform: Sereno's model, Fennema and Thompson's method, and Ogata and Sato's method.

5.3. *Sereno's Neural-network Model*

Sereno (1986, 1987, 1993) modeled the second stage of Adelson and Movshon's (1982) hypothesis as a network that connects the V1 cell array to the MT cell array. The connection is represented as a modification of our inverse Hough transform that links DS complex cells and motion-detection cells, as follows.

Sereno's V1 cells respond selectively to 1-D velocities and are arranged as the (θ, V_{1D}) array. The array is the same as our (θ, τ) DS complex cell array, excluding the $t_d/2$ coefficient [equation (6)]. In contrast, Sereno's MT cells, which detect the stimulus' 2-D motion, are arranged as a polar representation of our (τ_x, τ_y) motion-detection cell array, i.e. as the (ϕ, V_{2D}) orthogonal array with the relationship of $\phi = \tan^{-1}(\tau_y/\tau_x)$ and $V_{2D} = (2/t_d)\sqrt{(\tau_x^2 + \tau_y^2)}$.

Sereno modeled the second stage as a neural network that connects a V1 cell at (θ, V_{1D}) to all MT cells lying on the curve $V_{1D} = V_{2D}\cos(\phi - \theta)$ in the (ϕ, V_{2D}) array [Fig. 3.2(a) of Sereno (1993)]. The curve giving the connections is a representation of our elementary inverse Hough transform (Appendix A.2) in the (ϕ, V_{2D}) array.

This model accounts for the perceptual phenomena: direction and speed acuity, motion coherency, motion transparency, and misestimation of plaid motion.

Sereno's model, however, has two problems. The first is that Sereno does not give an algorithm for the detection of 1-D velocities of oriented components by the V1 cells, i.e. for the first stage. The second problem is the (ϕ, V_{2D}) arrangement of the MT cell array. A moving dot stimulus activates a MT cell, in the array, which detects the dot's 2-D motion. In contrast, a stationary dot causes activation in all MT cells along the array's $V_{2D} = 0$ coordinate. This activation, indicating that the stationary dot cannot be detected by a specific MT cell, is not perhaps plausible neurophysiologically. In our (τ_x, τ_y) arrangement, this stationary dot activates a motion-detection cell at $(\tau_x = 0, \tau_y = 0)$.

Replacing the τ in equation (5) and equation (12) and (τ_x, τ_y) in equation (14) with $\log_a \tau$ and $(\log_a \tau_x, \log_a \tau_y)$ allows us to represent these parameters on a log scale in the same way as Sereno's representation of V_{1D} and V_{2D}.

5.4. *Fennema and Thompson's Method*

The method presented by Fennema and Thompson (1979) also has two stages corresponding to those of Adelson and Movshon (1982).

The first stage uses the gradient scheme (Limb & Murphy, 1975) to measure the (θ, V_{1D}) 1-D velocities of oriented components within a stimulus that moves with (V_x, V_y) 2-D motion. Each V_{1D} speed is obtained by dividing the temporal gradient dI/dt by the respective spatial gradient dI/dx of the oriented component (I is the light intensity). Mapping these velocities in a (θ, V_{1D}) array gives a sine wave that satisfies the third form of equation (7).

To extract this wave for detecting the (V_x, V_y) 2-D motion, the second stage uses the same representation of

our inverse Hough transform in the (ϕ, V_{2D}) array as Sereno's model.

This model has three physiological problems. The division used in the gradient scheme cannot be implemented by neuron easily. We did not use it. In addition, the velocity detection process is sensitive to noise because of the gradient scheme, which is not plausible neurophysiologically. Our process is robust to noise (Section 3.6). Finally, since this method uses the same (ϕ, V_{2D}) arrangement as Sereno's model, it suffers from the same associated problem.

5.5. Ogata and Sato's Method

The method presented by Ogata and Sato (1991) is based on scalar motion sensors (Watson & Ahumada, 1985). It uses the inverse Hough transform to combine the sensor outputs for detecting 2-D motion.

The 1-D velocity of an oriented component with orientation θ is coded in a ratio f_t/f_s; f_t is the temporal frequency of a scalar-motion-sensor response, and the sensor prefers a sinusoidal grating with θ orientation and f_s spatial frequency. A stimulus moving with (V_x, V_y) 2-D motion causes a sine wave [equation (19)] composed of activated scalar motion sensors over a $(\theta, f_t/f_s)$ array (Watson & Ahumada, 1985):

$$f_t/f_s = V_x \cos\theta + V_y \sin\theta. \quad (19)$$

The wave corresponds to our sine waves [equation (10)] composed of activated DS complex cells over the (θ, τ) array. To detect the (V_x, V_y) 2-D motion, Ogata and Sato (1991) extracted this wave using an inverse Hough transform that is obtained by replacing the τ, τ_{x0}, and τ_{y0} of our transform [equation (A4) in Appendix A] with f_t/f_s, V_x, and V_y.

This method has two physiological problems. The Fourier transform—used for the conversion to the spatio-temporal frequency domain—cannot be implemented by neurons easily. Our cell model is described using synaptic functions (Section 2.4), in the real, or non-Fourier, domain. Second, this method cannot accurately detect the 2-D motion of isolated stimuli, such as single dots, because the Fourier components of such stimuli is small. This is inconsistent with neurophysiology (Section 2.1 and Section 4.2.2). Our cell model detects the 2-D motion of isolated stimuli, including single dots (Fig. 6B).

The method proposed by Heeger (1987) and Grzywacz *et al.* (1990) (Section 5.2) also uses the Fourier transform. Hence, it suffers from the same associated problem as this method.

6. DISCUSSION

6.1. Simple-cell Arrangement in Layer 4B

In Section 2.2 and Fig. 19, we proposed that, in layer 4B of the hypercolumns, NDS simple cells are arranged as the (ρ, θ) array and DS simple cells are arranged three-dimensionally as the (ρ, θ) array with a depth arrangement of τ. Based on the arrangements, we predicted the perpendicular crossing between the orientation and ocular-dominance columns.

This section shows that these arrangements and this perpendicular crossing are supported by neurophysiological observations using optical imaging and autoradiography.

6.1.1. The perpendicular crossing

Using optical imaging, Obermayer and Blasdel (1993) observed that the iso-orientation bands (or orientation columns) in area V1 of monkeys tend to intersect the borders of ocular dominance columns at roughly perpendicular angles. Further, using the autoradiographic method combining [^{14}C]2-deoxyglucose and [^{3}H]proline, Hubel, Wiesel and Stryker (1978) observed the roughly perpendicular crossing between the orientation and ocular-dominance columns in area V1 of monkeys.

These observations support our prediction of the perpendicular crossing. They also support our (ρ, θ) arrangement of NDS and DS simple cells indirectly, because the crossing results from the arrangement (Fig. 19).

6.1.2. The (ρ, θ) cell arrangement

Using optical imaging, Obermayer and Blasdel (1993^{++}) reported that 48% of area V1 consists of "linear zones". In these zones the orientation preferences change linearly along straight axes, remaining constant along the perpendicular axes and forming parallel iso-orientation bands. The straight axis corresponds to our θ coordinate, and the perpendicular axis to our ρ coordinate. Hence, this linear zone is consistent with our (ρ, θ) arrangement of NDS and DS simple cells (Section 6.3). We suggest that the linear zone is an observation of our (ρ, θ) arrangement in layer 4B. The predicted cell arrangement along the ρ coordinate, where preferences for bar location should change linearly along the coordinate, has not been validated previously, to our knowledge.

6.2. Tests for Validating the Cell Model

In our cell model, we make three assumptions. The first is the Hough transform processed in NDS simple cells [equation (4)], through which an NDS simple cell detects a line composed of activated LGN cells. The second assumption is the sequential processing by LGN cells, NDS and DS simple cells, and DS complex cells [equations (2, 4, 5, and 12)], through which the 2-D motion of a moving stimulus is transformed into a sine wave composed of activated DS complex cells [equation (10)]. The third assumption is the inverse Hough transform processed in motion-detection cells [equation (14)], through which a motion-detection cell extracts the sine wave.

In the sections that follow, we propose three tests that can be used to confirm these transforms, based on single and twin microelectrodes (Kuffler *et al.*, 1984) and optical imaging (Blasdel & Salama, 1986; Grinvald, Lieke, Frostig, Gilbert & Wiesel, 1986). Detailed testing procedures, together with predicted cell responses

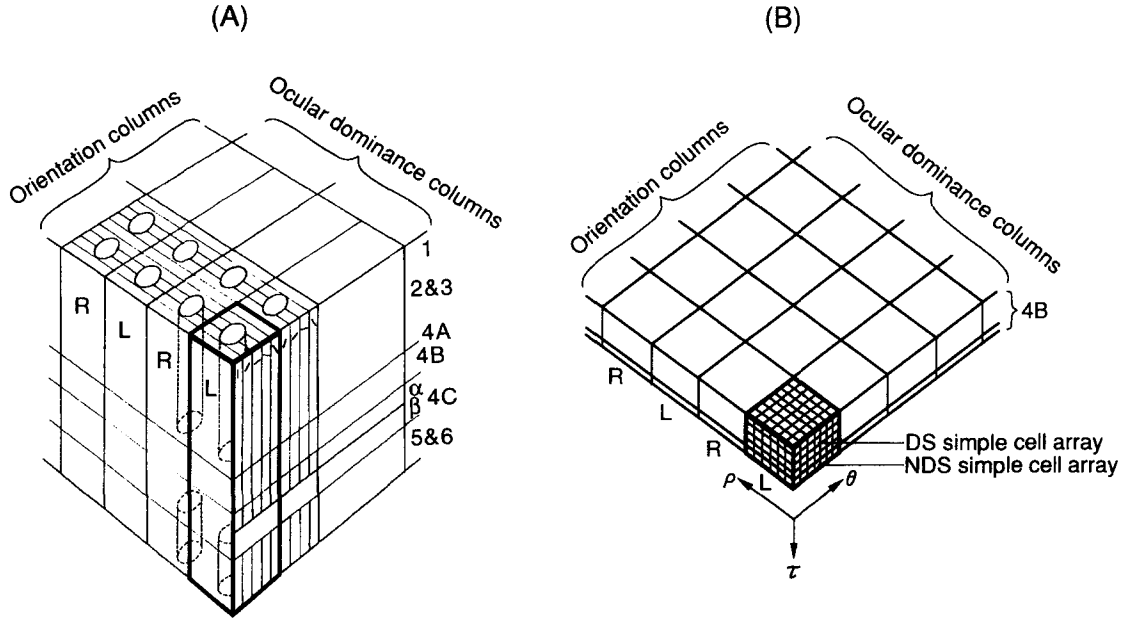

FIGURE 19. (A) Hypercolumns taken from Livingstone and Hubel (1984), which constitute a regular structure over area V1 of the cortex. We marked a hypercolumn with bold lines. R and L denote the ocular dominance columns (or ocular dominance bands) of the right and left eyes. (B) Proposed arrangement of NDS and DS simple cells in layer 4B of the hypercolumns, based on the presence of the simple cells in this layer (Section 2.1). Each cell in the layer of a hypercolumn belonging to the left eye, for example, is depicted as a cube. We propose that NDS simple cells are arranged as the (ρ, θ) array in the lower part. We also propose that, in the upper part, DS simple cells are arranged three-dimensionally as the (ρ, θ) array with a depth arrangement of τ. This proposal for the (ρ, θ, τ) arrangement is based on the observations by Hubel and Wiesel (1977), Humphrey and Norton (1980), and Humphrey, Skeen and Norton (1980): "the orientation and location preferences of simple cells change roughly linearly across area V1, remaining constant along the depth axis". We predict that the array's ρ coordinate is the arrangement of ocular dominance columns. Cells lie along the columns, with the same-eye ocular dominance and the same ρ location preference. The preferred θ orientations shift gradually from cell to cell. We also predict that the θ coordinate is the arrangement of orientation columns (or iso-orientation bands). Cells lie along the columns, with the same θ orientation preference and with preferred ρ locations shifting gradually from cell to cell. The two types of column cross perpendicularly, due to the (ρ, θ) orthogonal coordinates of the Hough plane. This perpendicular crossing was suggested by Hubel and Wiesel (1974). [A similar (ρ, θ) arrangement of NDS simple cells was predicted by Okajima (1986) using the Radon transform, and suggested by Blasdel (1992b), Obermayer and Blasdel (1993), and Blasdel and Obermayer (1994) based on the Hough transform.]

occurring in them, are described for neurophysiologists to conduct the tests.

6.2.1. Single microelectrodes

Tests using single microelectrodes can confirm that these transforms are processed in individual cells.

6.2.1.1. Hough transform. The test steps for confirming this transform are as follows: (1) position the electrode on an NDS simple cell; (2) stimulate the cell with stationary dots at different (x, y) locations; and (3) depict the cell responses as a map whose address is a dot location.

A line composed of the cell's responses should occur in the (x, y) map (Fig. 20A). This indicates that the cell extracts the line. Hence, by measuring the linear response pattern, we can confirm that the cell processes the Hough transform [equation (4)].

To detail the test, using stationary bar stimuli, we can measure the ρ_0 foot and θ_0 angle of the pattern directly. Measure the location and orientation of a bar preferred by the cell. This location and orientation should give the pattern's foot and angle.

6.2.1.2. Sequential processing. The test steps are as follows: (1) position the electrode on a DS complex cell; (2) stimulate the cell with dots moving with different (V_x, V_y) 2-D motions; and (3) depict the cell responses as a map whose address is the 2-D motion of a dot.

A line composed of the cell's responses should occur in the (V_x, V_y) map (Fig. 20B). This indicates that the complex cell extracts the line. Hence, by measuring the linear response pattern, we can confirm that through the sequential processing the cell extracts the constraint line.

Using moving bar stimuli, we can measure the V_{1D0} foot and θ_0 angle of the pattern directly. Measure the 1-D velocity and orientation of a bar preferred by the cell. They should give the pattern's foot and angle.

6.2.1.3. Inverse Hough transform. The test steps are as follows: (1) position the electrode on a motion-detection cell; (2) stimulate the cell with bars moving with different (V_{1D}, θ) 1-D velocities; and (3) depict the cell responses as a map whose address is the 1-D velocity of a bar.

A sine wave composed of the cell's responses should occur in the (θ, V_{1D}) map (Fig. 20C). This indicates that the motion-detection cell extracts the wave. Hence, by measuring the sinusoidal response pattern, we can confirm that the cell processes the inverse Hough transform [equation (14)], because the wave is equivalent to the sinusoidal firing pattern [equation (10)] extracted through the transform.

Using moving dot stimuli, we can measure the V_{1D0}

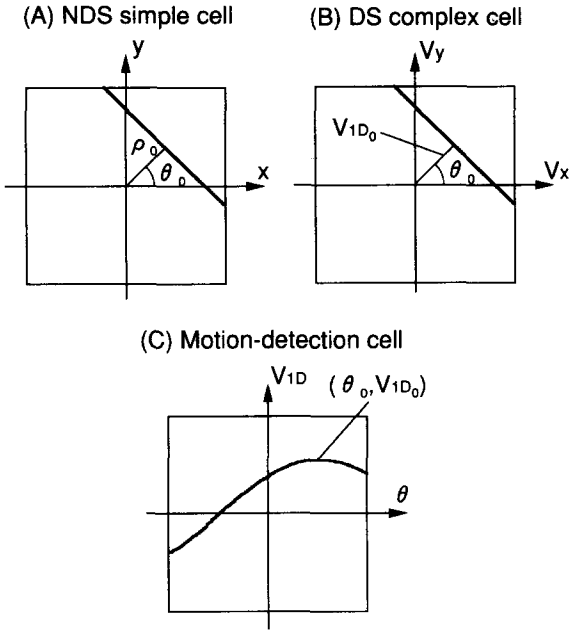

FIGURE 20. Prediction of cell response patterns. (A) The responses of an NDS simple cell [equation (4)] at (ρ_0, θ_0) for stationary dot stimuli with different (x, y) locations are depicted as a map whose address is a dot location. A line composed of the cell's responses, $\rho_0 = x\cos\theta_0 + y\sin\theta_0$, occurs in the (x, y) map. The line's ρ_0 foot and θ_0 angle coincide with the cell's coordinates. (B) The responses of a DS complex cell [equation (12)] at (θ_0, τ_0) for dot stimuli moving with different (V_x, V_y) 2-D motions are depicted as a map whose address is the 2-D motion of a dot. A line composed of the cell's responses, $V_{1D0} = V_x\cos\theta_0 + V_y\sin\theta_0$, occurs in the (V_x, V_y) map. The line is a constraint line [equation (7)] whose V_{1D0} foot and θ_0 angle are given by the cell's coordinates as $V_{1D0} = 2\tau_0/t_d$. (C) The responses of a motion-detection cell [equation (14)] at (τ_{x0}, τ_{y0}) for bar moving with different (V_{1D}, θ) 1-D velocities are depicted as a map whose address is the 1-D velocity of a bar. A sine wave composed of the cell's responses, $t_d V_{1D}/2 = \tau_{x0}\cos\theta + \tau_{y0}\sin\theta$, occurs in the (θ, V_{1D}) map. The V_{1D0} amplitude and θ_0 phase of the wave are given by the cell's coordinates, with the relationship of $V_{1D0} = (2/t_d)\sqrt{(\tau_{x0}^2 + \tau_{y0}^2)}$ and $\theta_0 = \tan^{-1}(\tau_{y0}/\tau_{x0})$.

amplitude and θ_0 phase of the pattern directly. Measure the speed and direction of a dot preferred by the cell. They should give the pattern's amplitude and phase.

Finally, we show that these predicted response patterns are supported by neurophysiological observations. First, the linear response pattern of an NDS simple cell (Fig. 20A) is the elongated, excitatory receptive field of the cell [Fig. 15A(ii)]. Hence, the observation of this field in actual simple cells (Jones & Palmer, 1987a$^+$,b$^+$) supports our linear pattern. Next, as shown in Fig. 21A, the linear response pattern of a DS complex cell (Fig. 20B) is a synthesis of the bimodal direction-tuning curves (Fig. 14A) for dots moving with all 2-D motions. Hence, the observation of these curves in actual DS complex cells (Section 4.2.3.1) supports our linear pattern. Finally, as shown in Fig. 21B, the sinusoidal response pattern of a motion-detection cell (Fig. 20C) is a synthesis of the bimodal direction-tuning curves (Fig. 14B) for bars moving with all 1-D velocities. Hence, the observation of these curves in actual motion-detection cells (Section 4.2.3.2) supports our sinusoidal pattern.

6.2.2. Twin microelectrodes

Tests using twin microelectrodes can confirm that the three transforms are processed across the corresponding cell arrays.

6.2.2.1. Hough transform. The test steps are as follows: (1) insert the twin electrodes into an NDS simple cell array; (2) measure and calculate the location (x_c, y_c) of a stationary dot stimulus [Fig. 22A(i)]; and (3) stimulate with this stationary dot.

The twin electrodes should respond selectively to the dot's location [Fig. 22A(ii)]. Hence, by measuring this selective response, we can confirm that the Hough transformation of the dot is executed across the NDS simple cell array.

6.2.2.2. Sequential processing. The test steps are as follows: (1) insert the electrodes into a DS complex cell array; (2) measure and calculate the 2-D motion (V_{xc}, V_{yc}) of a moving dot stimulus [Fig. 22B(i)]; and (3) stimulate with this moving dot.

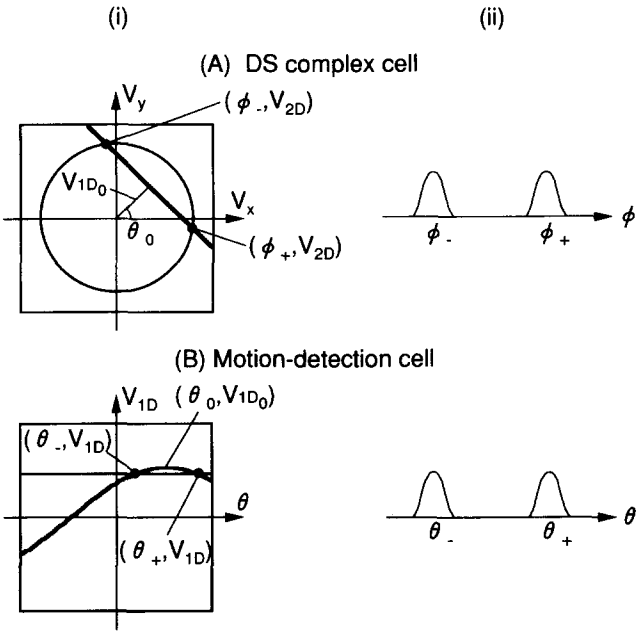

FIGURE 21. The bimodal direction-tuning curves (Fig. 14) of DS complex cells and motion-detection cells are a different representation of the linear and sinusoidal response patterns of the cell types (Fig. 20B and C). A(i) The linear response pattern (Fig. 20B) of a DS complex cell in the (V_x, V_y) map. We assume a slice of the map along a circle with radius V_{2D}. The intersections of the pattern and the circle are (ϕ_-, V_{2D}) and (ϕ_+, V_{2D}) in the polar representation. A(ii) The bimodal direction-tuning curve of the cell (Fig. 14A), which occurs for dot stimuli moving with a 2-D motion equal to the V_{2D} radius. This curve coincides with the slice above. The ϕ_- and ϕ_+ directions of the bimodal tunings are the intersections' ϕ coordinates. Hence, a synthesis of such tuning curves for dots moving with all 2-D motions is the linear response pattern. B(i) The sinusoidal response pattern (Fig. 20C) of a motion-detection cell in the (θ, V_{1D}) map. We assume a slice of the map along a line that is parallel to the θ axis and has a coordinate V_{1D}. The intersections of the pattern and the line are (θ_-, V_{1D}) and (θ_+, V_{1D}). B(ii) The bimodal direction-tuning curve of the cell (Fig. 14B), which occurs for bar stimuli moving with a 1-D velocity equal to the V_{1D} coordinate. This curve coincides with the slice above. The θ_- and θ_+ directions of the bimodal tunings are the intersections' θ coordinates. Hence, a synthesis of such tuning curves for bars moving with all 1-D velocities is the sinusoidal response pattern.

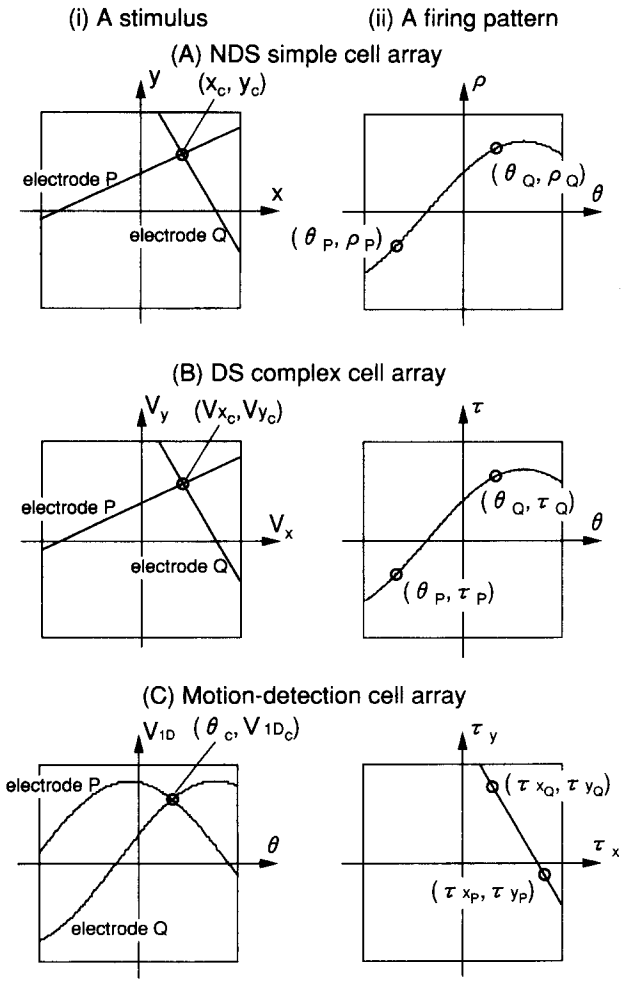

FIGURE 22. Prediction of stimuli that cause the cell firing patterns passing through twin electrodes (P and Q) in the respective cell array (A–C). A(i) The (x_c, y_c) location of a stationary dot stimulus is determined as the intersection of the linear response patterns (Fig. 20A) at the individual electrodes. A(ii) Through the Hough transform, the stimulus causes a sinusoidal firing pattern that passes through the twin electrodes, (θ_P, ρ_P) and (θ_Q, θ_Q), in the cell array. B(i) The (V_{xc}, V_{yc}) 2-D motion of a moving dot stimulus is determined as the intersection of the linear response patterns (Fig. 20B) at the individual electrodes. B(ii) Through the sequential processing [equations (2, 4, 5, and 12)], the stimulus causes a sinusoidal firing pattern that passes through (θ_P, τ_P) and (θ_Q, τ_Q) in the cell array. C(i) The (θ_c, V_{1Dc}) 1-D velocity of a moving bar stimulus is determined as the intersection of the sinusoidal response patterns (Fig. 20C) at the individual electrodes. C(ii) Through the inverse Hough transform, the stimulus causes a linear firing pattern that passes through (τ_{xP}, τ_{yP}) and (τ_{xQ}, τ_{yQ}) in the cell array.

The twin electrodes should respond simultaneously and selectively to the 2-D motion [Fig. 22B(ii)]. Hence, by measuring this simultaneous, selective response, we can confirm that the conversion (of the dot's motion to a sinusoidal pattern) through the sequential processing is executed across the DS complex cell array.

6.2.2.3. Inverse Hough transform. The test steps are as follows: (1) insert the electrodes into a motion-detection cell array; (2) measure and calculate the 1-D velocity (θ_c, V_{1Dc}) of a moving bar stimulus [Fig. 22C(i)]; and (3) stimulate with this moving bar.

The twin electrodes should respond simultaneously and selectively to the 1-D velocity [Fig. 22C(ii)]. Hence, by measuring this simultaneous, selective response, we can confirm that the inverse Hough transformation is executed across the motion-detection cell array.

6.2.3. Optical imaging

Optical imaging enables us to observe firing patterns occurring over cell arrays. This imaging has been developed extensively (Blasdel & Salama, 1986; Grinvald *et al.*, 1986; Bonhoeffer & Grinvald, 1991; Blasdel, 1992a,b; Bartfeld & Grinvald, 1992; Obermayer & Blasdel, 1993; Bonhoeffer & Grinvald, 1993; Shoham, Gottesfeld & Grinvald, 1993).

By observing three types of firing patterns using this imaging, we can confirm our transforms. The first is a sinusoidal firing pattern in the NDS simple cell array [Fig. 6B(ii)], caused by a dot stimulus. This pattern indicates that the Hough transformation of the dot is processed over the NDS simple cell array. The second is a sinusoidal firing pattern in the DS complex cell array [Fig. 6B(iv)], caused by a moving dot stimulus. This pattern indicates that the conversion through the sequential processing, above, is processed over the DS complex cell arrays. The third is a linear firing pattern in the motion-detection cell array [e.g. Fig. 6A(v)], caused by a moving bar stimulus. This pattern indicates that the inverse Hough transformation is processed over the motion-detection cell array.

However, since the cell arrangement across the visual cortex is distorted, it is difficult to evaluate the linearity and waveform of these patterns correctly.

We present tests for confirming the transforms without evaluating the linearity and waveform. Therefore, the tests are not affected by the cortex distortion.

6.2.3.1. Hough transform. The test steps are as follows: (1) stimulate with a group of stationary dot stimuli [Fig. 23A(i)], then confirm that a group of firing patterns intersect at a point; and (2) stimulate with a (ρ_0, θ_0) stationary bar, then observe a firing spot [e.g. Fig. 6A(ii)].

The spot's location should coincide with the point of intersection [Fig. 23A(ii)]. Hence, by measuring this coincidence, we can confirm that the Hough transform is processed over the NDS simple cell array.

6.2.3.2. Sequential processing. The test steps are as follows: (1) stimulate with a group of moving dot stimuli [Fig. 23B(i)], then confirm that a group of firing patterns intersect at a point; and (2) stimulate with a bar moving with (V_{1D0}, θ_0) 1-D velocity, then observe a firing spot [e.g. Fig. 6A(iv)].

The spot's location should coincide with the point of intersection [Fig. 23B(ii)]. Hence, by measuring this coincidence, we can confirm that the conversion through the sequential processing, above, is processed over the DS complex cell array.

6.2.3.3. Inverse Hough transform. The test steps are as follows: (1) stimulate with a group of moving bar stimuli [Fig. 23C(i)], then confirm that a group of firing patterns intersect at a point; and (2) stimulate with a dot moving with (V_{x0}, V_{y0}) 2-D motion, then observe a firing spot [e.g. Fig. 6B(v)].

The spot's location should coincide with the point of intersection [Fig. 23C(ii)]. Hence, by measuring this

coincidence, we can confirm that the inverse Hough transform is processed over the motion-detection cell array.

Finally, we compare the tests using microelectrode and optical-imaging: because electrodes measure responses that reflect the neuronal network of a cell, electrodes provide measurements that are independent of the distortion in the cell arrangement across the cortex. However, the measurements are localized at the electrodes and do not cover the cell array. In contrast, optical imaging can observe the cell firing patterns over the visual cortex. However, because the observation is affected by the distortion, it is difficult to evaluate the patterns' waveforms correctly. Furthermore, the depth resolution of optical-imaging apparatus is poor (e.g. Bonhoeffer & Grinvald, 1993; Bartfeld & Grinvald, 1992). Hence, combining these two types of test allows us to validate the Hough and inverse Hough transforms and the sequential processing.

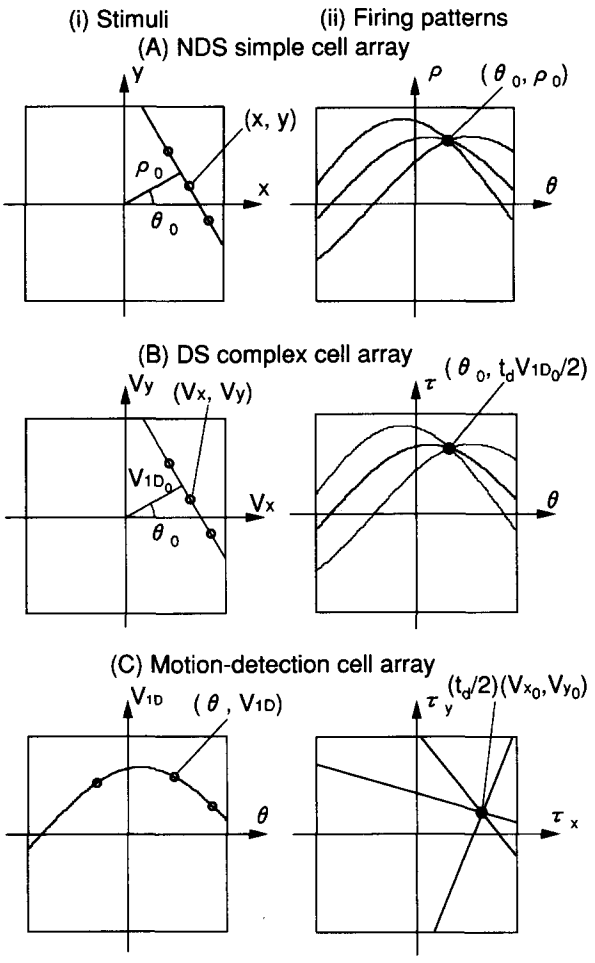

FIGURE 23. Prediction of firing patterns over the respective cell array (A–C) caused by three types of stimulus group. A(i) A group of stationary dot stimuli on a bar (θ_0, ρ_0), whose (x, y) locations satisfy the relationship $\rho_0 = x\cos\theta_0 + y\sin\theta_0$. A(ii) Through the Hough transform, the stimuli cause a group of sinusoidal firing patterns over the NDS simple cells array, which intersect at (θ_0, ρ_0). B(i) A group of moving dot stimuli whose (V_x, V_y) 2-D motions lie on a constraint line $V_{1D0} = V_x\cos\theta_0 + V_y\sin\theta_0$. B(ii) Through the sequential processing [equation (2, 4, 5, and12)], the stimuli cause a group of sinusoidal firing patterns over the DS complex cell array, which intersect at (θ_0, $t_dV_{1D0}/2$). C(i) A group of bar stimuli moving with (V_{x0}, V_{y0}) 2-D motion, whose (θ, V_{1D}) 1-D velocities lie on a sinusoidal wave $V_{1D} = V_{x0}\cos\theta + V_{y0}\sin\theta$. C(ii) Through the inverse Hough transform, the stimuli cause a group of linear firing patterns over the motion-detection cell array, which intersect at ($t_d/2$)(V_{x0}, V_{y0}).

6.3. *Linear and Pinwheel-like Firing Patterns*

This section shows that a group of bar stimuli, which move with differing orientations but at a constant speed V_{1D}, cause linear and pinwheel-like firing patterns over the the modeled cell arrays. These resemble the patterns occurring over the actual cell arrays for a group of rectangular wave gratings that move with the same orientations and speed as the bar group. (We note that the grating is a group of parallel bars.)

In the NDS simple cell array, the bar group causes a stack of linear firing patterns in the (ρ, θ) array (Fig. 24A). This stack resembles the linear zones (Obermayer & Blasdel, 1993) that were observed in area V1 of macaque monkeys for the grating group using optical imaging. The iso-orientation bands constituting the zone correspond to these linear patterns.

In a (ρ, θ) slice of the DS simple cell array at a τ coordinate of $t_dV_{1D}/2$, the same stack of linear firing patterns as in the NDS simple cell array is caused by the bar group.

In the DS complex cell array, a linear firing pattern (Fig. 24B) parallel to the θ axis and having a τ coordinate of $t_dV_{1D}/2$ is caused by the bar group. This pattern has not been observed previously, to our knowledge.

Finally, in the motion-detection cell array, a group of linear firing patterns (Fig. 24C) tangential to a circle with radius $t_dV_{1D}/2$ are caused by the bar group. When the V_{1D} speed is small, this pattern group becomes a pinwheel-like pattern intersecting at the origin of the array. Orientation preferences rotate through 360 deg for one revolution about the origin. This pinwheel-like pattern resembles that observed in area MT of owl monkeys for the grating group using optical imaging (Malonek, Tootell & Grinvald, 1993; Tootell, Malonek & Grinvald, 1992). We note that motion-detection cells are present in area MT of macaque monkeys (Section 2.1).

7. CONCLUSION

We proposed that the five types of cells on the magnocellular visual pathway constitute a function hierarchy to detect 2-D motion from a moving stimulus (Fig. 1; Section 2). LGN cells first introduce a time delay to transform a spatio-temporal parameter (the 1-D velocity) into a spatial parameter (the displacement between the lagged and nonlagged images). Then, NDS and DS simple cells perform a Hough transform and Reichardt's spatio-temporal correlation to detect the 1-D velocities of oriented components within the stimulus. Accumulating these velocities, a group of DS complex cells along a sine wave fire over the cell array. The wave indicates all possible 1-D velocities in the stimulus, and its amplitude and phase correspond to the speed and direction of the 2-D motion. Finally, motion-detection

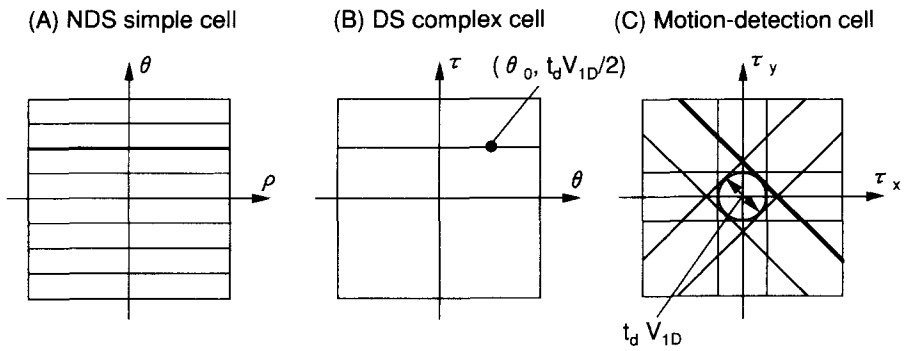

FIGURE 24. Prediction of firing patterns in the respective cell array (A–C) caused by a group of bar stimuli moving with different orientations but a constant speed V_{1D}. (A) We assume a bar moving with a θ_0 orientation and the V_{1D} speed. The position (ρ, θ_0) of an NDS simple cell detecting the bar moves along the ρ coordinate with the speed, then resulting in a linear firing pattern (a bold line). The bar group, thus, causes a stack of such linear firing patterns for the bars moving with all orientations. (B) The moving bar with the θ_0 orientation activates a DS complex cell at $(\theta_0, t_d V_{1D}/2)$ shown as a bold dot. The bar group thus causes a line composed of such activated DS complex cells. The line is parallel to the θ axis and has the τ coordinate of $t_d V_{1D}/2$. (C) The moving bar with the θ_0 orientation causes a line composed of activated motion-detection cells in the (τ_x, τ_y) array (a bold line). The line is inclined by the θ_0 orientation and tangential to a circle with radius $t_d V_{1D}/2$. The bar group, thus, causes a group of such lines tangential to the circle.

cells perform the inverse Hough transform to extract the wave. As a result of this sequential processing, a stimulus moving with (V_x, V_y) 2-D motion causes activation in a motion-detection cell at $(t_d/2)(V_x, V_y)$, where t_d is the fixed time delay of lagged LGN cells. From this cell's coordinates, the 2-D motion is determined.

We modeled the responses of these five cell types as a series of formulas [equations (2, 4, 5, 12, and 14)] that represent three types of synaptic functions in neurons: the postsynaptic excitation and inhibition; the synaptic transmission efficiency; and a multiplication-like function (Section 2). These formulas represent the neuronal network linking retinal cells and motion-detection cells in area MT.

The modeled cells detected 2-D motion from a variety of continuously and apparently moving stimuli, including dots, straight lines, curves, edges, and plaid patterns (Sections 3, 4.2, and 4.5). They also detected the 2-D motions from two moving stimuli within a receptive field separately. This is consistent with motion transparency in psychophysiology. They further detected the 2-D motion of a line with terminators.

The modeled cells are consistent with neurophysiology, as follows.

All the modeled cells exhibit the same selectivities to traditionally used bar stimuli as actual cells (Section 4.1). They reflect the grain and field responses to the movement of random-dot textures in actual cells (Section 4.4). The modeled DS simple and complex cells and motion-detection cells also reflect the response to apparent motion in actual cells (Section 4.5).

Our DS complex cells exhibit the same direction and orientation selectivities to the three combinations of stimuli as the Component and type I cells in areas V1 and MT (Section 4.2). Our motion-detection cells exhibit the same selectivities as the Pattern and type II cells in area MT.

Our NDS simple cells and modified NDS simple cells account for the two receptive-field structures that are characteristic of actual simple cells and resemble the 2-D even and odd Gabor functions (Section 4.3).

Finally, our (ρ, θ) arrangement of NDS and DS simple cells is supported by neurophysiological observations (Section 6.1).

The modeled cells accounted for Adelson and Movshon's two-stage hypothesis neurophysiologically (Section 5.1). The first stage is executed in the sequential processing by LGN cells, DS and NDS simple cells, and DS complex cells. The second stage is executed in the motion-detection cells. The IOC solution of the hypothesis is equivalent to our inverse Hough transform processed in motion-detection cells.

The modeled cells, which are described using synaptic functions of neurons and consistent with neurophysiology, resolve the physiological inconsistency in the previous models (Sections 5.2–5.5).

Using microelectrodes and optical imaging, we proposed three tests for confirming the cell model's validity (Section 6.2).

We suggested that the linear zones observed in area V1 of macaque monkeys using optical imaging occur in the NDS and DS simple cell arrays, and also suggested that the 360 deg type of pinwheel-like pattern observed in area MT of owl monkeys occurs in the motion-detection cell array (Section 6.3).

This is, to our knowledge, the first model of the neurophysiological process by which cells on the magnocellular visual pathway detect local 2-D motion.

REFERENCES

Adelson, E. H. & Bergen, J. R. (1985). Spatiotemporal energy models for the perception of motion. *Journal of the Optical Society of America, A, 2*, 284–299.

Adelson, E. H. & Movshon, J. A. (1982). Phenomenal coherence of moving visual patterns. *Nature, 300*, 523–525.

Albright, T. D. (1984). Direction and orientation selectivity of neurons in visual area MT of the macaque. *Journal of Neurophysiology, 52*, 1106–1130.

Albright, T. D., Rodman, H. R. & Gross, C. G. (1986). Type II MT neurons show pattern-motion direction selectivity. *Neuroscience Abstracts*, *12*, 1369.

Baker, C. L. Jr (1988). Spatial and temporal determinants of directionally selective velocity preference in cat striate cortex neurons. *Journal of Neurophysiology*, *59*, 1557–1574.

Baker, C. L. Jr & Cynader, M. S. (1986). Spatial receptive-field properties of direction-selective neurons in cat striate cortex. *Journal of Neurophysiology*, *55*, 1136–1152.

Baker, C. L. Jr & Cynader, M. S. (1988). Space–time separability of direction selectivity in cat striate cortex neurons. *Vision Research*, *28*, 239–246.

Ballard, D. H. & Brown, C. M. (1982). *Computer vision*. Englewood Cliffs, N.J.: Prentice-Hall.

Ballard, D. H., Hinton, G. E. & Sejnowski, T. J. (1983). Parallel visual computation. *Nature*, *306*, 21–26.

Barlow, H. B. (1980). Critical limiting factors in the design of the eye and visual cortex. *Proceedings of the Royal Society of London B*, *212*, 1–34.

Barlow, H. B. & Levick, W. R. (1965). The mechanism of directionally selective units in rabbit's retina. *Journal of Physiology*, *178*, 477–504.

Bartfeld, E. & Grinvald, A. (1992). Relationships between orientation-preference pinwheels, cytochrome oxidase blobs, and ocular-dominance columns in primate striate cortex. *Proceedings of the National Academy of Science, U.S.A.*, *89*, 11905–11909.

Blasdel, G. G. (1992a). Differential imaging of ocular dominance and orientation selectivity in monkey striate cortex. *Journal of Neuroscience*, *12*, 3115–3138.

Blasdel, G. G. (1992b). Orientation selectivity, preference, and continuity in monkey striate cortex. *Journal of Neuroscience*, *12*, 3139–3161.

Blasdel, G. & Obermayer, K. (1994). Putative strategies of scene segmentation in monkey visual cortex. *Neural Networks*, *7*, 865–881.

Blasdel, G. G. & Salama, G. (1986). Voltage-sensitive dyes reveal a modular organization in monkey striate cortex. *Nature*, *321*, 579–585.

Bonhoeffer, T. & Grinvald, A. (1991). Iso-orientation domains in cat visual cortex are arranged in pinwheel-like patterns. *Nature*, *353*, 429–431.

Bonhoeffer, T. & Grinvald, A. (1993). The layout of iso-orientation domains in area 18 of cat visual cortex: Optical imaging reveals a pinwheel-like organization. *Journal of Neuroscience*, *13*, 4157–4180.

Boothe, R. G., Greenough, W. T., Lund, J. S. & Wrege, K. (1979). A quantitative investigation of spine and dendrite development of neurons in visual cortex (area 17) of macaca nemestrina monkeys. *Journal of Comparative Neurology*, *186*, 473–490.

Borst, A. & Egelhaaf, M. (1989). Principles of visual motion detection. *Trends in the Neurosciences*, *12*, 297–306.

Burke, D. & Wenderoth, P. (1993). The effect of interactions between one-dimensional component gratings on two-dimensional motion perception. *Vision Research*, *33*, 343–350.

Casagrande, V. A. (1994). A third parallel visual pathway to primate area V1. *Trends in the Neurosciences*, *17*, 305–310.

Casasent, D. & Krishnapuram, R. (1987). Curved object location by Hough transformations and inversions. *Pattern Recognition*, *20*, 181–188.

Daugman, J. G. (1985). Uncertainty relation for resolution in space, spatial frequency, and orientation optimized by two-dimensional visual cortical filters. *Journal of the Optical Society of America, A*, *2*, 1160–1169.

Duda, R. O. & Hart, P. E. (1972). Use of the Hough transformation to detect lines and curves in pictures. *Communications ACM*, *15*, 11–15.

Duda, R. O. & Hart, P. E. (1973). *Pattern recognition and scene analysis*. New York: Wiley.

Duffy, C. J. & Wurtz, R. H. (1991a). Sensitivity of MST neurons to optic flow stimuli. 1. A continuum of response selectivity to large-field stimuli. *Journal of Neurophysiology*, *65*, 1329–1345.

Duffy, C. J. & Wurtz, R. H. (1991b). Sensitivity of MST neurons to optic flow stimuli. 2. Mechanisms of response selectivity revealed by small-field stimuli. *Journal of Neurophysiology*, *65*, 1346–1359.

Edelstyn, N. M. J. & Hammond, P. (1988). Relationship between cortical lamination and texture sensitivity in complex neurones of the striate cortex in cats. *Journal of Comparative Neurology*, *278*, 397–404.

Egelhaaf, M. & Borst, A. (1993). A look into the cockpit of the fly: Visual orientation, algorithms, and identified neurons. *Journal of Neuroscience*, *13*, 4563–4574.

Emerson, R. C., Citron, M. C., Vaughn, W. J. & Klein, S. A. (1987). Nonlinear directionally selective subunits in complex cells of cat striate cortex. *Journal of Neurophysiology*, *58*, 33–65.

Emerson, R. C., Bergen, J. R. & Adelson, E. H. (1992). Directionally selective complex cells and the computation of motion energy in cat visual cortex. *Vision Research*, *32*, 203–218.

Enroth-Cugell, C. & Robson, J. G. (1966). The contrast sensitivity of retinal ganglion cells of the cat. *Journal of Physiology*, *187*, 517–552.

Fennema, C. L. & Thompson, W. B. (1979). Velocity determination in scenes containing several moving objects. *Computer Graphics and Image Processing*, *9*, 301–315.

Ferrera, V. P. & Wilson, H. R. (1990). Perceived direction of moving two-dimensional patterns. *Vision Research*, *30*, 273–287.

Ferster, D. & Lindström, S. (1983). An intracellular analysis of geniculo-cortical connectivity in area 17 of the cat. *Journal of Physiology*, *342*, 181–215.

Fitzpatrick, D., Lund, J. S. & Blasdel, G. G. (1985). Intrinsic connections of macaque striate cortex: Afferent and efferent connections of lamina 4C. *Journal of Neuroscience*, *5*, 3329–3349.

Gilbert, C. D. & Wiesel, T. N. (1981). Laminar specialization and intracortical connections in cat primary visual cortex. In Schmitt, F. O., Worden, F. O., Adelman, G. & Dennis, S. G. (Eds), *The organization of the cerebral cortex* (pp. 163–191). Cambrige, Mass.: MIT Press.

Grinvald, A., Lieke, E., Frostig, R. D., Gilbert, C. D. & Wiesel, T. N. (1986). Functional architecture of cortex revealed by optical imaging of intrinsic signals. *Nature*, *324*, 361–364.

Grzywacz, N. M. & Yuille, A. L. (1990). A model for the estimate of local image velocity by cells in the visual cortex. *Proceedings of the Royal Society of London B*, *239*, 129–161.

Gulyas, B., Orban, G. A., Duysens, J. & Maes, H. (1987). The suppressive influence of moving textured backgrounds on responses of cat striate neurons to moving bars. *Journal of Neurophysiology*, *57*, 1767–1791.

Hammond, P. (1978). Directional tuning of complex cells in area 17 of the feline visual cortex. *Journal of Physiology*, *285*, 479–491.

Hammond, P. & MacKay, D. M. (1977). Differential responsiveness of simple and complex cells in cat striate cortex to visual texture. *Experimental Brain Research*, *30*, 275–296.

Hammond, P. & Reck, J. (1980). Influence of velocity on directional tuning of complex cells in cat striate cortex for texture motion. *Neuroscience Letters*, *19*, 309–314.

Hammond, P. & Smith, A. T. (1983). Directional tuning interactions between moving oriented and textured stimuli in complex cells of feline striate cortex. *Journal of Physiology*, *342*, 35–49.

Hartveit, E. & Heggelund, P. (1993). The effect of acetylcholine on the visual response of lagged cells in the cat dorsal lateral geniculate nucleus. *Experimental Brain Research*, *95*, 443–449.

Heeger, D. J. (1987). Model for the extraction of image flow. *Journal of the Optical Society of America, A*, *4*, 1455–1471.

Henry, G. H. (1977). Receptive field classes of cells in the striate cortex of the cat. *Brain Research*, *133*, 1–28.

Henry, G. H., Harvey, A. R. & Lund, J. S. (1979). The afferent connections and laminar distribution of cells in the cat striate cortex. *Journal of Comparative Neurology*, *187*, 725–744.

Hildreth, E. H. & Koch, C. (1987). The analysis of visual motion: From computational theory to neuronal mechanisms. *Annual Review of Neuroscience*, *10*, 477–533.

Hough, P. V. C. (1962). Method and means for recognizing complex patterns. U.S. Patent 3069654.

Hubel, D. H. & Livingstone, M. S. (1987). Segregation of form, color, and stereopsis in primate area 18. *Journal of Neuroscience*, *7*, 3378–3416.

Hubel, D. H. & Wiesel, T. N. (1959). Receptive fields of single neurones in the cat's striate cortex. *Journal of Physiology*, *148*, 574–591.

Hubel, D. H. & Wiesel, T. N. (1961). Integrative action in the cat's lateral geniculate body. *Journal of Physiology*, *155*, 385–398.

Hubel, D. H. & Wiesel, T. N. (1962). Receptive fields, binocular interaction and functional architecture in the cat's visual cortex. *Journal of Physiology*, *160*, 106–154.

Hubel, D. H. & Wiesel, T. N. (1968). Receptive fields and functional architecture of monkey striate cortex. *Journal of Physiology*, *195*, 215–243.

Hubel, D. H. & Wiesel, T. N. (1972). Laminar and columnar distribution of geniculo-cortical fibers in the macaque monkey. *Journal of Comparative Neurology*, *146*, 421–450.

Hubel, D. H. & Wiesel, T. N. (1974). Sequence regularity and geometry of orientation columns in the monkey striate cortex. *Journal of Comparative Neurology*, *158*, 267–294.

Hubel, D. H. & Wiesel, T. N. (1977). Functional architecture of macaque monkey visual cortex. *Proceedings of the Royal Society of London B*, *198*, 1–59.

Hubel, D. H., Wiesel, T. N. & Stryker, M. P. (1978). Anatomical demonstration of orientation columns in macaque monkey. *Journal of Comparative Neurology*, *177*, 361–380.

Humphrey, A. L. & Norton, T. T. (1980). Topographic organization of the orientation column system in the striate cortex of the tree shrew (tupaia glis): 1. Microelectrode recording. *Journal of Comparative Neurology*, *192*, 531–547.

Humphrey, A. L. & Weller, R. E. (1988). Functionally distinct groups of X-cells in the lateral geniculate nucleus of the cat. *Journal of Comparative Neurology*, *268*, 429–447.

Humphrey, A. L., Skeen, L. C. & Norton, T. T. (1980). Topographic organization of the orientation column system in the striate cortex of the tree shrew (tupaia glis): 2. Deoxyglucose mapping. *Journal of Comparative Neurology*, *192*, 549–566.

Jones, J. P. & Palmer, L. A. (1987a). The two-dimensional spatial structure of simple receptive fields in cat striate cortex. *Journal of Neurophysiology*, *58*, 1187–1211.

Jones, J. P. & Palmer, L. A. (1987b). An evaluation of the two-dimensional Gabor filter model of simple receptive fields in cat striate cortex. *Journal of Neurophysiology*, *58*, 1233–1258.

Kawakami, S. & Okamoto, H. (1992). A model for intracortical connections of hypercolumn 6: Circle detection cell and connections of prestriate cells. Technical Report NC92-47 of the IEICE (pp. 21–28) (in Japanese).

Kawakami, S. & Okamoto, H. (1993). A model for neuronal network linking retinal and motion-detection cells in area MT. In *1993 Annual Conference of the Japanese Neural Network Society* (pp. 162–163) (in Japanese).

Kawakami, S. & Okamoto, H. (1995). How local image velocity is detected by cells on the magnocellular pathway of the visual cortex. Transaction J78-D-II of the IEICE (pp. 147–157) (in Japanese).

Kawakami, S., Okamoto, H. & Hasegawa, F. (1991). A model for intracortical connections of hypercolumn 2: Mathematical structures on intracortical connections. Technical Report NC91-104 of the IEICE (pp. 43–50) (in Japanese).

Kawakami, S., Okamoto, H. & Morita, T. (1992). A model for intracortical connections of hypercolumn 3: Correlation filterings and direction selectivity cells. Technical Report NC92-13 of the IEICE (pp. 89–96) (in Japanese).

Kuffler, S., Nicholls, J. G., & Martin, A. R. (1984). *From neuron to brain*. Sunderland: Sinauer Assoc.

Lagae, L., Raiguel, S. & Orban, G. A. (1993). Speed and direction selectivity of macaque middle temporal neurons. *Journal of Neurophysiology*, *69*, 19–39.

Leventhal, A. G., Rodieck, R. W. & Dreher, B. (1981). Retinal ganglion cell classes in the old world monkey: Morphology and central projections. *Science*, *213*, 1139–1142.

Limb, J. O. & Murphy, J. A. (1975). Estimating the velocity of moving images in television signals. *Computer Graphics and Image Processing*, *4*, 311–327.

Livingstone, M. S. & Hubel, D. H. (1984). Anatomy and physiology of a color system in the primate visual cortex. *Journal of Neuroscience*, *4*, 309–356.

Livingstone, M. S. & Hubel, D. H. (1988). Segregation of form, color, movement, and depth: Anatomy, physiology, and, perception. *Science*, *240*, 740–749.

Lund, J. S. & Boothe, R. G. (1975). Interlaminar connections and pyramidal neuron organization in the visual cortex, area 17, of the macaque monkey. *Journal of Comparative Neurology*, *159*, 305–334.

Lund, J. S., Lund, R. D., Hendrickson, A. E., Bunt, A. H. & Fuchs, A. F. (1976). The origin of efferent pathways from the primary visual cortex, area 17, of the macaque monkey as shown by retrograde transport of horseradish peroxidase. *Journal of Comparative Neurology*, *164*, 287–304.

Malonek, D., Tootell, R. B. H. & Grinvald, A. (1992). Relationship of iso-direction and iso-orientation maps revealed by optical imaging in owl monkey area MT. *Neuroscience Abstracts*, *18*, 389.

Malonek, D., Tootell, R. B. H. & Grinvald, A. (1993). Optical imaging of orientation, direction and retinotopic organization in area MT of the owl monkey. *Neuroscience Abstracts*, *19*, 1500.

Marr, D. & Hildreth, E. (1980). Theory of edge detection. *Proceedings of the Royal Society of London B*, *207*, 187–217.

Maske, R., Yamane, S. & Bishop, P. O. (1985). Simple and B-cells in cat striate cortex. Complementarity of responses to moving light and dark bars. *Journal of Neurophysiology*, *53*, 670–685.

Mastronarde, D. N. (1987a). Two classes of single-input X-cells in cat lateral geniculate nucleus. 1. Receptive-field properties and classification of cells. *Journal of Neurophysiology*, *57*, 357–380.

Mastronarde, D. N. (1987b). Two classes of single-input X-cells in cat lateral geniculate nucleus. 2. Retinal inputs and the generation of receptive-field properties. *Journal of Neurophysiology*, *57*, 381–413.

Maunsell, J. H. R. & Newsome, W. T. (1987). Visual processing in monkey extrastriate cortex. *Annual Review of Neuroscience*, *10*, 363–401.

Maunsell, J. H. R. & Van Essen, D. C. (1983a). Functional properties of neurons in middle temporal visual area (MT) of macaque monkey. 1. Selectivity for stimulus direction, velocity and orientation. *Journal of Neurophysiology*, *49*, 1127–1147.

Maunsell, J. H. R. & Van Essen, D. C. (1983b). The connections of the middle temporal visual area in the macaque and its relationship to a hierarchy of cortical visual areas. *Journal of Neuroscience*, *3*, 2563–2586.

Maunsell, J. H. R., Nealey, T. A. & DePriest, D. D. (1990). Magnocellular and parvocellular contributions to responses in the middle temporal visual area (MT) of the macaque monkey. *Journal of Neuroscience*, *10*, 3323–3334.

Merigan, W. H. & Maunsell, J. H. R. (1993) How parallel are the primate visual pathways? *Annual Review of Neuroscience*, *16*, 369–402.

Mikami, A. (1991). Direction selective neurons respond to short-range and long-range apparent motion stimuli in macaque visual area MT. *International Journal of Neuroscience*, *61*, 101–112.

Mikami, A., Newsome, W. T. & Wurtz, R. H. (1986a). Motion selectivity in macaque visual cortex. 1. Mechanisms of direction and speed selectivity in extrastriate area MT. *Journal of Neurophysiology*, *55*, 1308–1327.

Mikami A., Newsome, W. T. & Wurtz, R. H. (1986b). Motion selectivity in macaque visual cortex. 2. Spatiotemporal range of directional interactions in MT and V1. *Journal of Neurophysiology*, *55*, 1328–1339.

Movshon, J. A., Thompson, I. D. & Tolhurst, D. J. (1978a). Spatial summation in the receptive fields of simple cells in the cat's striate cortex. *Journal of Physiology*, *283*, 53–77.

Movshon, J. A., Thompson, I. D. & Tolhurst, D. J. (1978b). Receptive field organization of complex cells in the cat's striate cortex. *Journal of Physiology*, *283*, 79–99.

Movshon, J. A., Adelson, E. H., Gizzi, M. S. & Newsome, W. T. (1985). The analysis of moving visual patterns. *Experimental Brain Research (Suppl.)*, *11*, 117–152.

Nealey, T. A. & Maunsell, J. H. R. (1994). Magnocellular and parvocellular contributions to the responses of neurons in macaque striate cortex. *Journal of Neuroscience*, *14*, 2069–2079.

Newsome, W. T., Mikami, A. & Wurtz, R. H. (1986), Motion selectivity in macaque visual cortex. 3. Psychophysics and physiology of apparent motion. *Journal of Neurophysiology*, *55*, 1340–1351.

Obermayer, K. & Blasdel, G. G. (1993). Geometry of orientation and ocular dominance columns in monkey striate cortex. *Journal of Neuroscience*, *13*, 4114–4129.

Ogata, M. & Sato, T. (1991). Motion perception model with interaction between spatial frequency channels. *Systems and Computers in Japan*, *22*, 207–214.

Okajima, K. (1986). A mathematical model of the primary visual cortex and hypercolumn. *Biological Cybernetics*, *54*, 107–114.

Okamoto, H, Kawakami, S. & Oka, K. (1994). A model for local image velocity detection on the magnocellular visual pathway. *Neuroscience Abstracts*, *20*, 838.

Perry, V. H., Oehler, R. & Cowey, A. (1984). Retinal ganglion cells that project to the dorsal lateral geniculate nucleus in the macaque monkey. *Neuroscience*, *12*, 1101–1123.

Reichardt, W. (1961). Autocorrelation. A principle for the evaluation of sensory information by the central nervous system. In Rosenblith, W. A. (Ed.), *Sensory communication* (pp. 303–317). New York: Wiley.

Reichardt, W. (1987). Evaluation of optical motion information by movement detectors. *Journal of Comparative Physiology*, *161*, 533–547.

Rodman, H. R. & Albright, T. D. (1987) Coding of visual stimulus velocity in area MT of the macaque. *Vision Research*, *27*, 2035–2048.

Rodman, H. R. & Albright, T. D. (1989). Single-unit analysis of pattern-motion selective properties in the middle temporal visual area (MT). *Experimental Brain Research*, *75*, 53–64.

Rubin, N. & Hochstein, S. (1993). Isolating the effect of one-dimensional motion signals on the perceived direction of moving two-dimensional objects. *Vision Research*, *33*, 1385–1396.

Saito, H. (1993). Hierarchical neural analysis of optical flow in the macaque visual pathway. In Ono, K. *et al.* (Eds), *Brain mechanisms of perception and memory* (pp. 121–140). New York: OUP.

Saito, H., Yukie, M., Tanaka, K., Hikosaka, K., Fukada, Y. & Iwai, E. (1986). Integration of direction signals of image motion in the superior temporal sulcus of the macaque monkey. *Journal of Neuroscience*, *6*, 145–157.

Saul, A. B. & Humphrey, A. L. (1990). Spatial and temporal response properties of lagged and nonlagged cells in cat lateral geniculate nucleus. *Journal of Neurophysiology*, *64*, 206–224.

Schiller, P. H., Finlay, B. L. & Volman, S. F. (1976). Quantitative studies of single-cell properties in monkey striate cortex: 1. Spatiotemporal organization of receptive fields. *Journal of Neurophysiology*, *39*, 1288–1319.

Schmid, A. & Bulthoff, H. (1988). Using neuropharmacology to distinguish between excitatory and inhibitory movement detection mechanisms in the fly calliphora erythrocephala. *Biological and Cybernetics*, *59*, 71–80.

Sereno, M. E. (1986). A neural model for the measurement of visual motion. *Journal of the Optical Society of America*, *A*, *3*, 72.

Sereno, M. E. (1987). Implementing stages of motion analysis in neural networks. *Proceedings of the Ninth Annual Conference of the Cognitive Science Society*, 405–416.

Sereno, M. E. (1993). *Neural computation of pattern motion*. Cambridge, Mass.: MIT Press.

Shoham, D. D., Gottesfeld, Z. & Grinvald, A. (1993). Comparing maps of functional architecture obtained by optical imaging of intrinsic signals to maps and dynamic patterns of cortical activity recorded with voltage-sensitive dyes. *Neuroscience Abstracts*, *19*, 1500.

Skottun, B. C., Grosof, D. H. & De Valois, R. L. (1988). Responses of simple and complex cells to random dot patterns: A quantitative comparison. *Journal of Neurophysiology*, *59*, 1719–1735.

Snowden, R. J. Treue, S. & Andersen, R. A. (1992). The response of neurons in areas V1 and MT of the alert rhesus monkey to moving random dot patterns. *Experimental Brain Research*, *88*, 389–400.

Spatz, W. B. (1977). Topographical organized reciprocal connections between area 17 and MT (visual area of superior temporal sulcus) in the marmoset *Callithrix jacchus*. *Experimental Brain Research*, *27*, 559–572.

Tanaka, K., Hikosaka, K., Saito, H., Yukie, M., Fukada, Y. & Iwai, E. (1986). Analysis of local and wide-field movements in the superior temporal visual areas of the macaque monkey. *Journal of Neuroscience*, *6*, 134–144.

Tanaka, K. & Saito, H. (1989). Analysis of motion of the visual field by direction, expansion/contraction, and rotation cells clustered in the dorsal part of the medial superior temporal area of the macaque monkey. *Journal of Neurophysiology*, *62*, 626–641.

Tootell, R. B. H., Malonek, D. & Grinvald, A. (1992). Optical imaging of orientation maps in V1, V2, and MT of new world monkeys. *Neuroscience Abstracts*, *18*, 389.

Torre, V. & Poggio, T. (1978). A synaptic mechanism possibly underlying directional selectivity to motion. *Proceedings of the Royal Society of London B*, *202*, 409–416.

Van Santen, J. P. H. & Sperling, G. (1984). Temporal covariance model of human motion perception. *Journal of the Optical Society of America*, *A*, *1*, 451–473.

Van Santen, J. P. H. & Sperling, G. (1985). Elaborated Reichardt detectors. *Journal of the Optical Society of America*, *A*, *2*, 300–321.

Wässle, H., Grunert, U., Rohrenbeck, J. & Boycott, B. (1990). Retinal ganglion cell density and cortical magnification factor in the primate. *Vision Research*, *30*, 1897–1911.

Watson, A. B. & Ahumada, A. J. Jr (1985). Model of human visual-motion sensing. *Journal of the Optical Society of America*, *A*, *2*, 322–341.

Welch, L. (1989). The perception of moving plaids reveals two motion-processing stages. *Nature*, *337*, 734–736.

Wilson, H. R. (1978). Quantitative characterization of two types of line-spread function near the fovea. *Vision Research*, *18*, 971–981.

Wörgötter, F. & Eysel, U. T. (1989). Axis of preferred motion is a function of bar length in visual cortical receptive fields. *Experimental Brain Research*, *76*, 307–314.

Yamane, S., Maske, R. & Bishop, P. O. (1985). Direction selectivity of simple cells in cat striate cortex to moving light bars. 2. Relation to moving dark bar response. *Experimental Brain Research*, *57*, 523–536.

Zeki, S. & Shipp, S. (1988). The functional logic of cortex connections. *Nature*, *335*, 311–317.

Acknowledgements—We thank Hirobumi Takanashi, Masao Hiyane, Shigeru Sato, Bunichi Oguchi, and Junich Tanahashi for their encouragement during this work. We also thank Fumi Hasegawa and Yusuke Yasukawa for their support with the Hough transform simulator, and Toshihiko Morita, Yasushi Inamoto, Takashi Aoki, and Takashi Uchiyama for their support with simulation tools. We thank Hideaki Saito, Noboru Sugie, and Keiji Tanaka for their suggestions regarding neurophysiology on local image motion detection, and Kotaro Oka and Shozo Fujita for their suggestions regarding physiology. Finally, we thank Yasushi Miyashita, Miyao Shiina, and Kazuo Asakawa for their support in the physiological surveys, and Norio Fujimaki, Rosemary Geary, and Jun Setoguchi for reviewing and editing the manuscript.

APPENDIX A

Hough and Inverse Hough Transforms

This Appendix derives the Hough transform [equation (4)] processed in NDS simple cells and the inverse Hough transform [equation (14)] processed in motion-detection cells. The Hough transform detects lines in the LGN cell array, and the inverse Hough transform detects sine waves in the DS complex cell array.

A.1. Hough transform

Figure A1(i) outlines the Hough transform from the (x, y) LGN cell array to the (θ, ρ) NDS simple cell array. The transform converts a line in the (x, y) array into a spot in the (θ, ρ) array. We express this transform as a formula.

We assume an LGN cell that fires at (x_i, y_i) with an intensity LGN(x_i, y_i). The cell activates a group of NDS simple cells along a sine wave, $\rho = x_i\cos\theta + y_i\sin\theta$, with the LGN$(x_i, y_i)$ intensity. This elementary Hough transform is expressed as

$$\mathrm{LGN}(x_i, y_i)\ \delta(\rho - x_i\cos\theta - y_i\cdot\sin\theta) \qquad \text{(A1)}$$

where the delta function $\delta(\zeta) = 1$ for $\zeta = 0$ and $\delta(\zeta) = 0$ for $\zeta \neq 0$.

Then, we assume a group of LGN cells that fire along a line $\rho_0 = x\cos\theta_0 + y\sin\theta_0$ with LGN(x, y) intensities. The LGN cell group activates an NDS simple cell at (θ_0, ρ_0) most intensively. This cell's

response is expressed as equation (A2) by accumulating the elementary Hough transformations over all LGN cells in the (x, y) array:

$$SC_{NDS}(\rho_0, \theta_0) = \sum_x \sum_y LGN(x, y)\ \delta(\rho_0 - x\cos\theta_0 - y\cdot\sin\theta_0). \quad (A2)$$

Thus, equation (4) has been derived.

We must accumulate this Hough transform within a rectangular receptive field [Fig. A2 (ii)]. The intensity of NDS simple cell responses [equation (A2)] decreases as the eccentricity of a line stimulus from the center of a circular receptive field [Fig. A2 (i)] increases. This is because the line segment within the circle (or the number of LGN cells to be accumulated by the Hough transform) reduces progressively.

To resolve this problem, we limit the accumulation to the rectangular receptive field. The field is inscribed in the circular receptive field and inclines by the cell's θ coordinate (i.e. its preferred orientation). With this limitation, the same number of LGN cells on the bold line [Fig. A2 (iii)] is accumulated, independent of the line's location and orientation. Hence, the optimal responses of NDS simple cells for line stimuli become constant and independent of their preferred locations and orientations. This is consistent with electrophysiology.

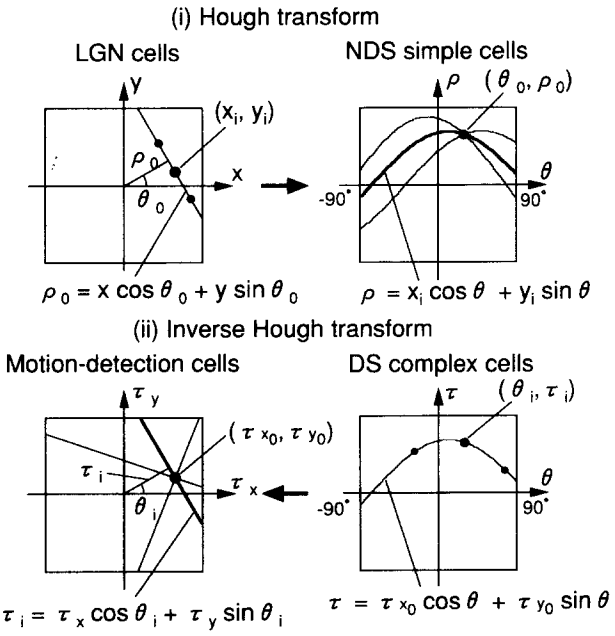

FIGURE A1. (i) The Hough transform from the (x, y) LGN cell array to the (θ, ρ) NDS simple cell array. Through the transform, an LGN cell at (x_i, y_i) activates a group of NDS simple cells along a sine wave $\rho = x_i\cos\theta + y_i\sin\theta$ over the (θ, ρ) array. This wave indicates the θ orientations and ρ locations of all possible lines passing through the (x_i, y_i) position. Then, if a group of LGN cells fire along a line $\rho_0 = x\cos\theta_0 + y\sin\theta_0$ over the (x, y) array, the sine waves activated by these LGN cells will intersect at a point (θ_0, ρ_0) in the (θ, ρ) array. The point indicates the line's θ_0 orientation and ρ_0 location. Hence, this Hough transform converts the line in the (x, y) array into the most intensive activation of a NDS simple cell at the point. This cell detects the line and is connected with all LGN cells on the line. The transform converts parallel lines in the (x, y) array into such firing peaks of NDS simple cells with the same θ coordinate. [Note that the transform does not include layer 4Cα cells which act as a relay (Section 2.1).] (ii) The inverse Hough transform from the (θ, τ) DS complex cell array to the (τ_x, τ_y) motion-detection cell array. The (θ, τ) and (τ_x, τ_y) arrays are mathematically equivalent to the (θ, ρ) and (x, y) arrays. This transform is the inverse operation of a Hough transform from the (τ_x, τ_y) array to the (θ, τ) array. A DS complex cell at (θ_i, τ_i) activates a group of motion-detection cells along a line $\tau_i = \tau_x\cos\theta_i + \tau_y\sin\theta_i$ over the (τ_x, τ_y) array. Then, if a group of DS complex cells fire along a sine wave $\tau = \tau_{x0}\cos\theta + \tau_{y0}\sin\theta$ over the (θ, τ) array, the lines activated by these complex cells will intersect at a point (τ_{x0}, τ_{y0}) in the (τ_x, τ_y) array. The point corresponds to the wave's $\sqrt{(\tau_{x0}^2 + \tau_{y0}^2)}$ amplitude and $\tan^{-1}(\tau_{y0}/\tau_{x0})$ phase. Hence, this inverse Hough transform converts the sine wave into the most intensive activation of a motion-detection cell at the point. This cell detects the wave and is connected with all DS complex cells on the wave. We note that the sinusoidal relationship between the θ and τ coordinates derives from the basic relationship [equation (7)] between the (V_{2D}, ϕ) 2-D motion and (V_{1D}, θ) 1-D velocity of a line (Section 2.3.1). This sine wave represents all possible 1-D velocities in a stimulus moving with the (V_{2D}, ϕ) 2-D motion.

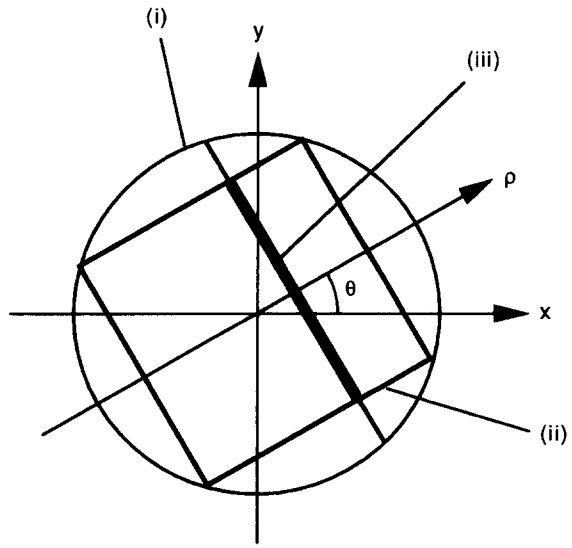

FIGURE A2. Three types of receptive field of cells. (i) Circular receptive field. (ii) Rectangular receptive field that is inscribed in the circular one and inclines by the cell's preferred orientation θ. Our Hough transform [equations (4) and (A2)] is accumulated within this rectangular field. (iii) Linear receptive field.

We notice that our modeled cells possess the three types of receptive-field (Fig. A2): NDS and DS simple cells [equation (4) and equation (5)] possess the linear receptive field [Fig. A2 (iii)]. The location and orientation of the field correspond to the cell's (ρ, θ) coordinates (Section 4.3.1). A DS complex cell [equation (12)] possesses the rectangular receptive field inclined by the cell's preferred orientation [Fig. A2 (ii)]. The field is a synthesis of the linear receptive fields of all DS simple cells that have the same orientation and 1-D velocity selectivities as the complex cell. Finally, a motion-detection cell [equation (14)] possesses the circular receptive field [Fig. A2 (i)] that is a synthesis of the rectangular receptive fields of DS complex cells with all orientation selectivities. The rectangular and circular fields of these cells are independent of the contrast polarity of stimuli.

A.2. Inverse Hough transform

Figure A1 (ii) outlines the inverse Hough transform from the (θ, τ) DS complex cell array to the (τ_x, τ_y) motion-detection cell array. The transform converts a sine wave in the (θ, τ) array into a spot in the (τ_x, τ_y) array. We express this transform as a formula.

We assume a DS complex cell that fires at (θ_i, τ_i) with $CC_{DS}(\theta_i, \tau_i)$ intensity. The cell activates a group of motion-detection cells along a line, $\tau_i = \tau_x\cos\theta_i + \tau_y\sin\theta_i$, with the $CC_{DS}(\theta_i, \tau_i)$ intensity. This elementary inverse Hough transform is expressed as

$$CC_{DS}(\theta_i, \tau_i)\ \delta(\tau_i - \tau_x\cos\theta_i - \tau_y\sin\theta_i). \quad (A3)$$

Then, we assume a group of DS complex cells that fire along a sine wave $\tau = \tau_{x0}\cos\theta + \tau_{y0}\sin\theta$ with $CC_{DS}(\theta, \tau)$ intensities. The DS complex cell group activates a motion-detection cell at (τ_{x0}, τ_{y0}) most intensively. This cell's response is expressed as equation (A4) by accumulating the elementary inverse Hough transformations over all DS complex cells in the (θ, τ) array:

$$MDC(\tau_{x0}, \tau_{y0}) = \sum_\theta \sum_\tau CC_{DS}(\theta, \tau)\ \delta(\tau - \tau_{x0}\cos\theta - \tau_{y0}\sin\theta). \quad (A4)$$

Thus, equation (14) has been derived.

APPENDIX B

Parameters for Computer Simulation

This Appendix shows the parameters used for computer simulations. We based the sizes of the receptive fields (Fig. A2) and cell

arrays (Figs 2 and 5) on physiological considerations and our model: We first determined the number of cells constituting the θ coordinate as 180 deg/10 deg = 18 cells, because the discrimination in θ orientation of actual V1 cells is about 10 deg. Next, we set the rectangular receptive field size to 23 × 23 cells, based on the cortical magnification factor and the interval between adjacent hypercolumns (Wässle, Grunert, Rohrenbeck & Boycott, 1990; Hubel *et al.*, 1978^{++}; Kawakami, Okamoto & Hasegawa, 1991). Then, the circular receptive field circumscribed to this square is a circle which is 31 cells in diameter. Hence, the (ρ, θ) NDS simple cell array is 23 × 18 cells, the (ρ, θ, τ) DS simple cell array is 23 × 18 × 23 cells, the (θ, τ) DS complex cell array is 18 × 23 cells, and the (τ_x, τ_y) motion-detection cell array is 23 × 23 cells.

The parameter s in equation (3) has the value 2, except in the simulations (Figs 15 and 16) where we used $s = 4$.

Finally, based on these parameters and the proposed connections in all types of modeled cell (Section 2.4), we estimated the number of each cell type's connections within a receptive field.

Each LGN cell [equation (2)] is effectively connected with $\pi[(6 + 1 + 6)/2]^2$ retinal cells because values of equation (3) with $s = 2$ are negligibly small for $\sqrt{(u^2 + v^2)} > 6$. Since a receptive field contains $\pi(31/2)^2$ LGN cells, the number of retinal cell to LGN cell connections is $\pi(13/2)^2 \times \pi(31/2)^2 = 1.0 \times 10^5$.

Each layer 4Cα cell is connected to one LGN cell. Thus, the number of LGN cell to layer 4Cα cell connections is $\pi(31/2)^2 = 754$.

Each NDS simple cell [equation (4)] is connected with 23 layer 4Cα cells on a line within the rectangular receptive field. Since the NDS simple cell array contains 23 × 18 cells, the number of such connections is 23 × 23 × 18 = 9522.

Each DS simple cell [equation (5)] is connected with a pair of lagged and nonlagged NDS simple cells with the same orientation selectivity. Since the DS simple cell array contains 23 × 18 × 23 cells, the number of such connections is 2 × 23 × 18 × 23 = 19,044.

Each DS complex cell [equation (12)] is connected to 23 NDS simple cells with the same orientation and 1-D velocity selectivities. Since the DS complex cell array contains 18 × 23 cells, the number of such connections is 23 × 18 × 23 = 9522.

Each motion-detection cell (equation 14) is connected with 18 DS complex cells on a sine wave. Since the motion-detection cell array contains 23 × 23 cells, the number of such connections is 18 × 23 × 23 = 9522.

By summing these numbers of connections in each cell type, the number of cell sequence connections in a receptive field is estimated to be $[2 \times (10 + 0.07 + 0.95) + 1.9 + 0.95 + 0.95] \times 10^4 = 2.6 \times 10^5$.